Naval Research Laboratory

Washington, DC 20375-5320

NRL/MR/6180--98-8157

Experimental Study of Fire Suppression with Water Mist 1. Small Gaseous Diffusion Flame

C.C. NDUBIZU

GEO-CENTERS, INC.
Rockville, Maryland

R. ANANTH
P.A. TATEM

Navy Technology Center for Safety and Survivability
Chemistry Division

April 15, 1998

REPORT DOCUMENTATION PAGE

Form Approved
OMB No. 0704-0188

1. AGENCY USE ONLY (*Leave Blank*)	2. REPORT DATE	3. REPORT TYPE AND DATES COVERED
	April 15, 1998	Interim/1995-1997

4. TITLE AND SUBTITLE

Experimental Study of Fire Suppression with Water Mist
1. Small Gaseous Diffusion Flame

5. FUNDING NUMBERS

61-6000-0-8

6. AUTHOR(S)

R. Ananth, P.A. Tatem, and C.C. Ndubizu*

7. PERFORMING ORGANIZATION NAME(S) AND ADDRESS(ES)

Naval Research Laboratory
Washington, DC 20375-5320

8. PERFORMING ORGANIZATION REPORT NUMBER

NRL/MR/6180--98-8157

9. SPONSORING/MONITORING AGENCY NAME(S) AND ADDRESS(ES)

Office of Naval Research
800 North Quincy Street
Arlington, VA 22217-5660

10. SPONSORING/MONITORING AGENCY REPORT NUMBER

11. SUPPLEMENTARY NOTES

*Geo Centers, Inc., Rockville, MD.

12a. DISTRIBUTION/AVAILABILITY STATEMENT

Approved for public release; distribution is unlimited.

12b. DISTRIBUTION CODE

13. ABSTRACT (*Maximum 200 words*)

This report presents a study of the relative contributions of latent heat, heat capacity effects and oxygen dilution in the water mist suppression of a gaseous diffusion flame. The work is motivated by the urgent need to find an alternative to the banned halogen-based fire suppressing agents. Water mist is a contending alternative agent especially in total flooding applications. A modified Wolfhard-Parker burner was used to establish a 2D methane-air diffusion flame. Drops in flame temperature were measured when various quantities of nitrogen, steam and water mist were added independently in a co-flow arrangement. Thermal images of the flames were also obtained using the Agema Thermovision ® Instrument. Both temperature and IR measurements show that water mist suppresses both the flame temperature and flame height. A simple model of the flame was used to estimate the heat generation and loss processes taking place in the flame when small amounts of various suppressants were added. The results of both experiments and the analysis show that in a co-flow arrangement, where small quantities of water mist are added to the diffusion flame, the effects of latent heat, heat capacity and oxygen dilution are all important. The report also shows that overall, the contributions of thermal cooling are slightly bigger than those of oxygen dilution.

14. SUBJECT TERMS

15. NUMBER OF PAGES

50

16. PRICE CODE

17. SECURITY CLASSIFICATION OF REPORT	18. SECURITY CLASSIFICATION OF THIS PAGE	19. SECURITY CLASSIFICATION OF ABSTRACT	20. LIMITATION OF ABSTRACT
UNCLASSIFIED	UNCLASSIFIED	UNCLASSIFIED	UL

NSN 7540-01-280-5500

Standard Form 298 (Rev. 2-89)
Prescribed by ANSI Std 239-18
298-102

CONTENTS

FIGURES

Experimental Study of Fire Suppression With Water Mist
1. Small Gaseous Diffusion Flame.

1.0 INTRODUCTION

The 1992 Copenhagen Amendment to the Montreal Protocol banned the production of Halon 1301 (CF_3Br), in developed countries, because of it's Ozone Depletion Potential (ODP). The U.S. Navy has approximately 1.4 million pounds of Halon 1301 in over 2200 systems on about 220 ships. The need to find an environmentally compatible alternative to Halon 1301 is, therefore, of particular interest to the U.S. Navy. Fine water mist shows promise as an alternative especially in total flooding applications. Water mist as a fire fighting agent has the following advantages:

- Water is readily available
- It is Nontoxic
- It has a Zero ODP
- It does not Generate Hydrogen Halide Acids
- It does not Cause Water Damage
- It is a non-abandon the space agent

The last two advantages are of particular interest to the U.S. Navy since the use of water mist will reduce the man hours required for clean-up after a fire. This fits well with the U.S. Navy's current desire to drastically reduce manning on ships of the next century.

Much of the earlier work on water mist concentrated on obtaining engineering design parameters that demonstrate that water mist can indeed be a good replacement for halon 1301 in various applications. These applications include spray and pool fires [1-3], aircraft cabins [4-7], shipboard machinery and engine room spaces [8-12] and shipboard accommodation spaces [13]. Some of these works are discussed in a recent review by Tatem et al [14]. To obtain an optimum design of a water mist system, however, one needs to understand the mechanisms by which water mist is so effective in suppressing fires.

The earliest investigations into the mechanisms of fire suppression by water mist include the works of Rasbash and coworkers in the 1960s [15- 17] and also that of Braidech et. al [18]. Water mist suppresses fire via the following mechanisms; (a) gas phase cooling, (b) fuel surface cooling, (c)

Manuscript approved March 9, 1998.

oxygen dilution, and (d) radiation attenuation. These mechanisms were discussed in a recent paper by Jackman et.al [19].

Gas Phase cooling: When water mist droplets evaporate in or near the fire they absorb latent heat of evaporation from the fire gases and form steam. The steam subsequently absorbs additional heat as it is heated up to the flame temperature since its heat capacity is about twice that of air. For each gram of water mist, one can estimate the contributions from sensible heat of the liquid, latent heat and higher heat capacity effects of the steam as follows:

Sensible heat for liquid: 336 J/g (Mist coming in at 20°C)
Latent Heat: 2260J/g
Higher heat capacity effects for Steam: 1127J/g (assume flame temperature about 1500 K).

In this estimate the specific heats of water , steam and air are 4.2 , 2.0 and 1.0 J/g, respectively [20]. From this estimate one can see that the sensible heat of the liquid is very small. However contributions from the heat capacity effects of steam is significant while that from latent heat is dominant. Gas phase cooling is the total heat absorbed from the flame gases by these three processes.

Surface cooling: In fuel surface cooling, mist droplets (or steam) get to the condensed fuel surface and absorb latent and/or sensible heat from it. This diminishes the heat available for fuel gasification and thereby reduces the rate of production of gaseous fuel. As the condensed fuel gasification rate goes down the heat release rate goes down.

Oxygen Dilution: When a droplet evaporates, its volume increases 1600 times. The vapor mixes with air (or fire gases inside the fire) and the oxygen volume or mole fraction goes down. The dilution of oxygen concentration affects the reaction rate by starving the fire of oxygen. If the fire is in an enclosed space, the oxygen concentration inside the enclosure falls rapidly with time because of consumption by fire and also because of displacement of what is left by the steady flow of mist and water vapor. Thus, the fire quickly dies of oxygen starvation. This is particularly true when the enclosed fire is large.

Radiation Attenuation: Fine water mist has been shown to significantly attenuate (by absorption and scattering) infrared radiation from fires. Log [21] , Coppalle et. al. [22] and Thomas[23] have published various methods of calculating the radiation attenuation by water mist sprays. Their results show that the amount of attenuation is a strong function of droplet diameter and droplet concentration. Radiation is the principal mode of heat transfer from the fire to the burning fuel or the virgin fuel surrounding the fire, especially if the fire is large. Therefore the presence of water mist in the fire would result in the attenuation of heat feedback to the burning surface and hence give rise to a reduction in the burning rate.

Most laboratory studies on the mechanisms of fire suppression by water mist have been of medium or large scale [15,16,24]. However, experimental observations have shown that small (less

turbulent) flames are more difficult to extinguish with water mist [25]. This difficulty has highlighted the need to understand the mechanisms of interaction of water mist with small flames. There are very few small scale laboratory studies which reveal the dynamics of water droplets in the fire flow field as well as shed more light on the physical and/or chemical processes taking place during the interaction of water droplets with the flame or burning solid. They usually involve small diffusion flames in the counter-flow or co-flow arrangement. The counter-flow configuration is more popular since it is more stable and easier to model; although it is less representative of a real fire. Recently, other configurations, like the Tsuji burner, which is also stable and easy to model, are gaining attention [26].

Seshadri [27] studied the extinction of methanol, heptane and wood in counterflow diffusion flames by the action of water mist. An oxidizing gas stream containing water droplets was directed downward onto the burning liquid or solid surface. Their results showed that the influence of the water droplets on the flame extinction is thermal only and no chemical effects were observed. Lately, Lentati and Chelliah [28] modeled the dynamics of water droplets and their effects on flame extinction in a methane - air counterflow diffusion flame. They showed that very small droplets ($\leq 10\mu m$) evaporate before they get to the flame while large droplets ($\geq 50\mu m$) penetrate through the flame. They concluded that the suppression effects were from gas phase cooling and oxygen dilution. In a related study, Li et.al [29] observed similar effects of droplet size in an experimental study with water mist impinging on a hot wall in a laminar stagnation flow with a flat premixed flame near the solid surface.

McCaffrey [30] studied the suppression of a hydrogen jet diffusion flame by water mist in a co-flow arrangement. Experiments were run with sprays of small droplets introduced with the hydrogen jet. They were interested in the feasibility of using water sprays to control off shore oil/gas blowout. Their results revealed the thermal effects of water and they also explored the effects of the spray on the flame lift-off. Recently, Ndubizu et. al. [31] studied the effects of large and small size droplets of water mist on the suppression of propane premixed and diffusion flames in co-flow arrangements. Their results reveal that oxygen dilution effects can be quite significant.

The current study will continue to investigate the contributions of the various water mist suppression mechanisms in a small diffusion flame. A better understanding of the relative importance of the various suppression mechanisms for a given fire scenario will be useful in obtaining optimum design parameters for suppressing the fire with water mist. A methane - air diffusion flame in the co-flow configuration will be utilized. This configuration is more representative of a real fire than the counter-flow configuration even though it is more difficult to stabilize when mist is introduced. The use of gaseous diffusion flame will simplify the problem by eliminating the complication resulting from fire feedback mechanism. Thus only gas phase cooling and oxygen dilution mechanisms will be studied in this flame.

This report presents only experimental work and does not include any results from a numerical simulation program being developed in conjunction with this work. It includes only the results obtained with two dimensional (2D) methane diffusion flames where water mist, steam and nitrogen

were introduced in the co-flow air. In earlier papers [32,33] we had reported on numerical studies of water mist interaction with similar flames where numerical predictions have been compared with experimental data. The specific objective of this report is to compare the effects of these three suppressants (nitrogen, steam and water mist) on the flame and deduce the relative contributions of the two suppression mechanisms.

2.0 EXPERIMENTAL

2.1 Experimental Setup

The Wolfhard - Parker burner [34] is a standard apparatus for obtaining a co-flow diffusion flame in the laboratory. To accommodate the introduction of water mist into the co-flow air, a modified version of this burner was built. Figure 1a is a schematic of the modified Wolfhard - Parker burner which is the key component of the experimental setup [35]. The fuel slot is 75mm long, 10mm wide and 150mm deep. It has two identical oxidizer channels 82mm long, 35mm wide and 150mm deep on each side. Beside each oxidizer channel is the mist generation chamber. Here, mist is generated with commercial low flow Delavan ® nozzles. A fraction of the mist generated in this chamber is entrained into the air stream through a slot on the air channel. The slot opening is adjustable to control the quantity of mist entrained into the air stream. The mist and air mix before the mixture flows into the combustion zone. To determine the mist flow rate, very fine screen is used to cover the channel for a given time. The mass of mist collected during this period gives a measure of the mist flow rate out of the air channel at steady state. To introduce steam instead of mist, an electrically heated fine screen is used to collect and evaporate the mist droplets before they exit from the air channel. The heat supply to the screen is adjusted to ensure that all the water droplets coming through the channel will evaporate. Hence the mass flow rates of water and steam are equal in corresponding tests.

The droplets are characterized using the Malvern particle analyser. The Instrument's laser beam is passed across the middle of the air channel exit (see Figure 1b) such that the beam hits the droplets as they exit the channel. The gap between the channel exit and the beam is 5mm. Table 1 shows the measured characteristics of the water mist as it leaves the air channels. All the nozzles are 60° solid cone spray nozzles. The measurements were made at the water pressure of 75 psi. (482.6KPa.), which is the pressure at which all the mist and steam tests were conducted. The droplet Sauter mean diameters (SMD) were measured with and without the flame and no significant difference was observed in the results. The droplet Sauter mean diameters increase with nozzle orifice size, from 29.0μm to 65.8μm. Information from the manufacturer indicates that for the same size nozzles the SMD of the droplets coming straight from the nozzles range from 66μm and 101μm at 80 psi. (551.6 KPa.) water pressure [36]. This implies that the droplets were further broken up in the mist generation chamber and perhaps more of the smaller size droplets were selectively entrained into the air stream. The droplet size distribution curves are shown in Appendix A.

The fuel slot is filled with fine clean sand which helps to obtain a near plug flow condition. For the experiments being reported here 99.9% pure methane is the fuel. Similarly, three layers of fine screen are used to produce a uniform air velocity profile in each channel. The flame entrains air and

suppressant from the two streams of air or air+ suppressant (mist, steam or nitrogen.) which sandwich the flame. In the current experiments, the average exit velocity of the fuel is 2.81cm/s and the average exit velocity of the air is 18.1 cm/s. A quartz glass shield, 47 cm long and 27 cm high (not shown in Figure 1a), sits on the burner on either side to protect the flame from any external disturbances. The flame temperature is measured with a 50μm diameter fine platinum/platinum -13%-rhodium thermocouple which goes in and out of the flame through a narrow slot on the flame shield. A pressurized steel tank supplies water to the nozzles through a series of filters. This helps to eliminate pressure fluctuations in the water line and ensures a steady flow of water mist into the co-flow air. The burner and the positioning instrument are both enclosed in a 2 by 2m enclosure to further reduce disturbances by surrounding air flow. A schematic of the experimental setup is shown in Figure 2 and a picture of the entire setup is shown in Figure 3..

2.2 Temperature Measurement with Thermocouple

To establish a 2D flame, methane of known flow rate is ignited and the co-flow air is turned on and set at the appropriate flow rate. The system is allowed to reach steady state before a suppressant (mist, steam or nitrogen) is introduced into the air stream. Then the thermocouple is positioned at any location to start measuring temperature. A computer controlled Newport 3D positioning instrument is used to move the thermocouple bead to any location in and around the flame where a temperature is measured. The thermocouple is allowed to stay at this location for a few seconds and then withdrawn. During this time, a set of temperature data (about 200 readings) is taken and the minimum, mean and maximum values are recorded. For the butt welded, 50μm diameter wire thermocouple , the time constant is about 30 milliseconds [37]. Therefore, the number of readings in a set and the data acquisition rate are set such that adequate time is allowed for the thermocouple to attain the temperature of the surrounding gas. At each height above the burner a continuous temperature mapping across the flame is obtained by moving the thermocouple in the Y direction (see Figure 1b) in 0.5mm increments. Since the flame is symmetrical about the center plane perpendicular to the Y axis, measurements are made in one half of the flame only. Flame temperature measurements show no significant variation in the X direction except near the edges. Therefore a single thermocouple at the center of the flame (in the X direction) was used to produce a mapping of temperatures in the flame by moving it across the flame (the Y direction) and along the height of the flame (Z direction).

The uncertainty in the mean temperature measurements is about ± 30 K for the tests without suppressant (base case), with nitrogen and with steam. For tests with mist, the uncertainty is about ±100K. This is because mist induced flow cause the flame to be unsteady especially close to the flame tip.

All the temperatures reported in this study have been corrected for thermocouple radiation. The temperature correction, ΔT is given by;

$$\Delta T=(\sigma d\frac{\varepsilon}{kNu})(T_m^4-T_\infty^4) \qquad (1)$$ where;

σ,ε, k, Nu and d are the Stefan-Boltzmann constant, thermocouple emissivity, thermal conductivity

of the air, Nusselt number and diameter of the thermocouple bead respectively. T_m is the measured temperature. We assume the thermocouple bead to be spherical and take Nu =2.0. The diameter of the sphere is taken to be 2.5 times the wire diameter as specified by the manufacturer [34]. ε= 0.15 (from manufacturer's handbook) and k = 0.09 w/m K. For example, for the 50μm thermocouple wire used in the present study, the radiation correction at 1800 K is +62 K.

An additional error is introduced in the measurements because of heat conduction. When the thermocouple bead is close to the center plane, part of the wire is exposed to the much higher peak temperature near the flame sheet and therefore measured temperature will be in error because of heat conduction between the high temperature region and the bead. To minimize this error we chose very small diameter thermocouple wire so as to minimize the cross sectional heat transfer area.

2.3 Temperature Measurement with the Infrared Scanner

Since the flame flickers when water mist is introduced, it is difficult to obtain a reliable point by point measurement of the flame temperature when mist was introduced. With the infrared scanner the flame could be frozen and instantaneous measurement made. The Agema Thermovision ® 870 was used to obtain infrared images of the various flames with and without suppressant. First the scanner was calibrated with a black body source at 1200 °C. For the flame (non-black body) the emissivity should be specified in order to obtain the temperature. Emissivity of the flame depends on several parameters, especially soot volume fraction. The emissivity of the current flames was obtained by matching the maximum flame temperature at the center plane in the base case (no suppressant) with the temperature at the same position measured with the thermocouple. It is then assumed that emissivity does not change much when mist or any other suppressant was added.

Images of the flames were obtained by viewing the flame along the X axis (see Figure 1b) . The scanner was positioned 120 cm away and focused at the center of the flame. Thermal images of the live flames were frozen and stored on diskettes and later analyzed with the CATS version 2.1 software.

3.0 THEORETICAL ANALYSIS

As shown in Figure 1, fuel and air flow out from the rectangular burner as two-dimensional jets and are ignited to form a diffusion flame. The flame entrains air due to shear and buoyancy. Fuel is ignited at the bottom of the flame and combustion is assumed complete at the top of the flame. Heat generated by combustion heats up the combustion products to the temperature T_h. Heat is also lost to the ambient from both sides of the flame by convection, conduction and radiation. The flame is considered as a starved reactor and the reaction is assumed to occur at an infinite rate relative to the rate of supply of oxygen to the combustion zone. Therefore, the rate of combustion is set equal to the rate of supply of oxygen. This assumption is not expected to be valid in the regions of extinction, where the reaction is the limiting step and Arrhenius effects are critical. Furthermore the rate of supply of air or oxygen to the combustion zone is determined by requiring that the fuel and oxygen are consumed in stoichiometric proportion.

When an inert suppressant is added to the air stream, it dilutes the oxygen to lower the heat generation rate per unit volume of the flame and also absorbs heat from the flame in the form of latent heat (in case of water mist) and sensible heat. As the combustion rate per unit volume of the flame is reduced by the suppressant, the flame spontaneously increases its height which is measured from the experiments. The increased flame height enables increased entrainment of air such that the fuel and oxygen react in stoichiometric proportions and reaction is complete within the combustion zone. This results in higher heat loss from the flame due to increased sensible heat and increased heat transfer area. The purpose of this analysis is to obtain an order of magnitude estimate of the relative effects of the various mechanisms and to establish approximate relationships between the degree of suppression of the flame temperature and the mass fraction of the suppressant in the feed by using macroscopic mass and energy balances across the entire height of the flame.

Figure 4 shows a schematic model of a symmetric flame of height, h, thickness 2w and width b. The fuel and the entrained mass enter the flame zone at temperatures T_0 and T_{a0}, respectively. It is assumed that fuel and entrained oxygen are consumed completely in stoichiometric proportions, and the entrained mist droplets evaporate completely. The rate of heat loss from the flame to the surrounding is represented by Newton's law of cooling with a constant overall heat transfer coefficient h_c. We consider the case where the entrained mass has the same composition of air and suppressant as in the surrounding . This is expected to be valid for the case with droplets small enough that they follow the streamlines of gas flow. We also neglected evaporation outside the flame.

The mass flow rate of fuel, m_f, and the stoichiometric oxidizer mass, m_e, which contains a suppressant of mass fraction, X_s^f, are related by stoichiometry; thus

$$m_f X_f \Delta H_f = m_e X_{on}(1-X_s)\Delta H_o \qquad (2);$$

where, X_f is the mass fraction of methane in the feed, X_{on} is the mass fraction of oxygen in normal air, (X_{on}=0.233). ΔH_f and ΔH_o are the heats of combustion per unit mass of fuel and oxygen, respectively. The entrainment rate given in equation (2) is for the flame (combustion) zone only.

The energy balance across the flame is given by

$$m_f C_{pf}(T_h - T_0) + m_e C_{pa}(T_h - T_{a0})(1-X_s) + m_e X_s L + m_e X_s C_{pv}(T_h - T_b)$$

$$+ m_e X_s C_{ps}(T_b - T_{a0}) + h_c hb(T_h - T_{a0}) = m_f X_f \Delta H_f \qquad (3)$$

where L, T_b, X_s, C_{ps} are the latent heat of vaporization, boiling point temperature, mass fraction and specific heat of the liquid suppressant, respectively. C_{pf}, C_{pa}, and C_{pv} are the specific heats of fuel, air and gaseous suppressant evaluated at their respective average of the inlet and flame temperatures. b is the width of the flame (along X axis in Figure 1b.) . By substituting equation (2) into equation (3) and using the measured values of h, T_0, T_{a0} and X_s, we eliminate m_e and solve for T_h. The final result is given in dimensionless form;

$$\Psi^h=\Psi^{ad}-(\Psi^{ad}-\Psi^a)N/[1+(\chi_f(1+X_s\omega))/(\chi_o(1-X_s))+N] \quad (4);$$ where

$$\Psi^h=(T_h-T_0)/T_0 \quad (5a);$$

$$\Psi^a=(T_0-T_{a0})/T_0 \quad (5b);$$

$$\chi_f=(X_f\Delta H_f)/(C_{pf}T_0) \quad (5c);$$

$$\chi_o=(X_{on}\Delta H_o)/(C_{pa}T_0) \quad (5d);$$

$$N=(h_c hb)/(m_f C_{pf}) \quad (5e);$$ and

$$\omega=(C_{pv}/C_{pa})-1 \quad (5f).$$

Ψ^{ad} is the adiabatic temperature, which is given by;

$$\Psi^{ad}=[(\chi_o-\Psi^a)-X_s(\chi_o-\Psi^a+(\Psi^a-\Psi^b)C_{ps}/C_{pa}+\Psi^b C_{pv}/C_{pa}+ L/C_{pa}T_0)]/[(1+\chi_o/\chi_f)+X_s(\omega-\chi_o/\chi_f)] \quad (6);$$

where

$$\Psi^b=(T_0-T_b)/T_0 \quad (7).$$

Equation (4) is the central result of the analysis. It shows that the flame temperature is lower than the adiabatic flame temperature because of heat loss to the surrounding. This loss is represented in the dimensionless number N (equation (5e)). N increases with the addition of a suppressant and this is accounted for by an increase in flame height h and an increase in the overall heat transfer coefficient h_c. Change in N due to increase in flame height is taken care of by using measured values of h. However h_c is assumed to be constant and evaluated from equation (3) using measured values of flame temperature for the case without a suppressant.

The primary effect of a suppressant is shown in equation (6), where the adiabatic flame temperature decreases roughly linearly with increasing value of X_s (for small mass fraction). The coefficient of X_s in the numerator shows the contributions due to oxygen dilution, specific heat of a liquid suppressant and the latent heat of vaporization. The term ω in the denominator represents the effect due to the specific heat of vapor.

The adiabatic flame temperature can be calculated more accurately by using the standard NASA-Lewis code[38], in place of equation (6) for stoichiometric combustion and given value of the mass fraction of various suppressants in liquid or gaseous form. Indeed, the theoretical results described in the next section are obtained from equation (4), where the adiabatic temperatures were calculated using the NASA code for T_0=623 K, T_{a0} = 298 K (for steam T_{a0}=373 K) measured in our experiments.

The effect of a suppressant on heat flux can be obtained by dividing equation (3) with $m_e \Delta H_f$ throughout, and eliminating m_e using equation (2) ;

$$h_c hb(T_h - T_{a0})/m_f \Delta H_f = X_f - (C_{pa}(T_h - T_{a0}) + rC_{pa}(T_h - T_0) +$$

$$X_s(\Delta C_p(T_h - T_{ao}) + \Delta C_p'(T_b - T_{a0}) + L - rC_{pa}(T_h - T_0)))/X_{on}(1 - X_s)\Delta H_o \qquad (8)$$

where;

$$r = (X_{on}\Delta H_o C_{pf})/\Delta H_f C_{pa}$$

$$\Delta C_p = C_{pv} - C_{pa}$$

and

$$\Delta C_p' = C_{ps} - C_{pv}.$$

It relates the fraction of total heat lost from the flame to the suppressant mass fraction and is consistent with the work of Beyler [39], who has recently generalized the well known fire point equation to gaseous fuels and included the effect of suppressants. Indeed our equation (8) collapses to equation 10 given by Beyler , if one substitutes X_f=1, $C_{pf} = C_{pa}$, $T_0 = T_b = T_{a0}$ into our equation (8) for a gaseous suppressant with identical specific heats for fuel and air. The unified fire point theory of Beyler , has been found to agree with experimental data on extinction of a variety of solid fuels as discussed recently by Tewarson in the 1995 SFPE handbook [40] . Furthermore, Ewing et.al. [41] calculated extinction concentrations for a variety of extinguishing materials using a similar approach and showed excellent agreement with experimental data for various fuels. Our calculations account for the heat loss from the flame sheet and generate a suppression curve for water mist for the present experimental study where methane fuel temperature at the burner exit is much higher than the ambient. The results for the drop in adiabatic flame temperature due to water mist are consistent with those reported by Ewing et al. [41]. The calculations are expected to be compared with the flame peak temperatures and the results are discussed in the next section.

4.0 RESULTS AND DISCUSSION

4.1 The methane - Air Diffusion ---the Base Case

Figure 5 is the temperature profile across the flame (the Y-direction in Fig. 1b) at various heights above the flame for the methane - Air diffusion flame with no suppressant. Since the flame is symmetrical about the center plane only one half of the profiles are shown. The profiles show the characteristic half M-shape with the peak temperature occurring near the flame sheet where the fuel and oxygen are supposed to react at the stoichiometric proportion. Close to the burner the peak temperature is observed about 1mm from the burner edge and its value increases slightly with height above the flame. As expected, the flame is coldest at the center plane which is the farthest point from the main source of heat, the flame sheet. The highest peak temperature is approximately 2000 K. This is consistent with what was measured by earlier workers. Smyth et.al. [42] measured about 1900K at a location 15mm above a slot burner. Working with a cylindrical burner, Mitchell et. al.[43] reported a temperature slightly less than 2000 K, at a location 24mm above the burner. Recently, McEnally and Pfefferle[44] reported a maximum temperature of about 2000 K in an axisymmetrical methane - Air diffusion flame. The adiabatic temperature of a methane - Air flame is about 2200 K [45].

4.2 The Effects of Suppressant on Flame Temperature

Table 2 shows the measured and predicted maximum flame temperatures at various levels of dilution of the combustion air with nitrogen. Also, shown in the table are the adiabatic flame temperatures predicted from equation (6) and also from the NASA code. It can be seen that at various dilution levels the analysis predicts the maximum flame temperature very well. The NASA code predicts a lower adiabatic flame temperature since it accounts for Gibbs equilibrium while the analysis does not. Furthermore, from Table 2 one can show that the measured and predicted (both adiabatic and non-adiabatic) drop in flame temperatures (as a result of oxygen dilution) are within 15% of each other. Therefore, the adiabatic calculations, which are simpler to perform, can give some useful insights as to the effects of physical flame suppressants.

For a mass fraction of the additional nitrogen in the range of 0.0 and 0.2 (Table 2) the maximum temperature dropped from about 1946 K to 1722 K. In the previous section we assumed that the reaction rate in the flame is infinite and the mixture is stoichiometric overall. Therefore, the observed suppression in flame temperature is caused principally by the thermal effects of oxygen dilution , since the heat capacity of nitrogen is about equal to that of air. This is unlike the case of mist or steam which will be discussed later.

Figure 6 shows three pictures of the methane - air diffusion flame with no suppressant (Base Case), 3% steam and 3% water mist. The pictures reveal the effects of mist on flame stability and the effects of steam (a diluent) and water mist on flame height. These effects will be discussed in detail in the next section.

Figures 7 to 15 show the measured temperature profiles half way across the flame for tests with three levels of water mist , steam and nitrogen addition. The three levels of dilution correspond to 0.034, 0.05 and 0.11 mass fraction of suppressant in the co-flow air and the corresponding droplet Sauter mean diameters are about 29μm, 54μm and 66μm. Figures 7- 9 show data measured at a height 10mm above the burner exit; while Figures 10-12 and 13-15 are for heights 30mm and 45mm respectively. The three heights chosen for measurement represent various regions of the flame as will be deduced later.

In Figures 7-15 one notes that for the same level of dilution, and at the various heights in the flame, water mist has a much higher effect on suppression than steam or nitrogen. Furthermore, Table 2 shows that a nitrogen mass fraction of 0.2 is required for the maximum flame temperature to drop from about 1946 K to about 1722K. However, Figures 7 - 9 show that about 0 .034 mass fraction of mist or 0.11 mass fraction of steam will produce a similar drop in flame temperature. Also by comparing the steam and nitrogen data in these Figures one could see that the suppression effect due to higher heat capacity of the steam is significant compared to that due to oxygen dilution. Finally, since it has been shown that the effects of higher heat capacity of steam contributes significantly to gas phase cooling , it follows that with water mist, the cooling effects from latent heat plus heat capacity may be bigger than that from oxygen dilution. This is shown more clearly in section 4.4.

In Figures 7-11 one observes marked departure from the M-shaped temperature profile with the introduction of water mist especially at higher heights in the flame. This effect of mist introduction increases with height above the burner as well as with increase in mist concentration in the co-flow air. It seems that the presence of mist introduces additional physical phenomena, which affect the stability of the flame and causes the flame to flicker. First, the droplets can exert drag on the surrounding air due to difference between the velocity of the droplet and the surrounding air, which can be 7 cm/s for a 50μm and 30 cm/s for a 100μm size. This creates disturbance in the flow pattern near the flame. Even when the droplets travel at nearly the same velocity as the air, the Stefan flow [46] of vapor from the surface of evaporating droplets can be very significant. As a droplet is carried by the air into the thermal boundary layer (few millimeters close to the flame front), it begins to evaporate. The efflux velocity of the vapor increases as the inverse of droplet diameter. For a droplet size of about 60 μm, the efflux velocity can be of the order of tens of centimeters per second relative to the droplet velocity. This additional momentum generated by evaporation can cause significant mixing and instabilities in the flow structure in the flame, especially at higher mass fraction of 0.11 where the droplet number density is estimated to be about 100 droplets per cubic centimeter. Secondly, the introduction of mist droplets in the co-flow stream may cause some random perturbation in the flow. Such a perturbation will tend to destabilize the flame and make it flicker. Furthermore the flow of mist from the nozzles may have random fluctuations. However, the use of pressurized water tank to supply water to the nozzles should ensure a constant water pressure and hence a steady flow of mist through the nozzles. In addition, the design of our apparatus attempts to confine the flow from the nozzles to separate chambers (see Figure 1a) and this should help to damp the effect of any mist flow fluctuation on the co-flow air jets. All of the above factors contribute to the flickering of the flame, which causes mixing of the hot and cold regions near the

flame front at any given distance above the burner exit. Indeed, this can be seen in Figures 8 , 9, 11 and 12.

Figure 16 shows the Infrared (IR) images of the flames with no suppressant, 3% nitrogen, 3% steam and 3% water mist. These images show (qualitatively) that in the test with nitrogen where oxygen dilution is the only mechanism, the flame temperature is suppressed less than in the tests with mist or steam where gas phase cooling plays an important additional role.

Because of flickering it is more difficult to determine the peak temperature at a given height when mist is introduced. As the flame moves, the thermocouple encounters various regions of the flame and this results in rapid changes in the temperature history measured with the thermocouple. Such changes in temperature with time in the base case tests and in tests with nitrogen are within the experimental error. At each point where temperature is measured, a maximum and mean values of the set of data are obtained. Thus the highest measured temperature at each height can be obtained and this temperature is assumed to approximate the peak temperature at that height.

4.3 Effects of Suppressant on Flame Height

There are several definitions of flame height in the literature. We consider the definition of flame height from Burke and Schumanns' theory [47] where flame height in a 2D diffusion flame is defined as the height above the burner where the two flame sheets come together at the plane of symmetry. The flame sheet is the narrow region where fuel and oxygen are supposed to react in stoichiometric proportion. At each height above the burner the location of the peak temperature is expected to be very close to the flame sheet location as illustrated in Figure 17. Therefore the height of the peak temperature along the center plane of symmetry is expected to be close to the flame height according to the above definition (see Figure 17). Recall from the temperature profile for the base case flame in Figure 5 that the temperature of the center plane of symmetry increases with height, reaches a peak and drops as the heat loss rate surpasses the heat generation rate and the plume region is approached.

Figure 18 is a plot of the peak temperature versus height for the flames with and without suppressant. The peak temperature rises (slightly) to a plateau and then drops off in the plume region. Figure 18 shows that in the base case flame (no suppressant) the flame height is close to 40mm. With nitrogen as the suppressant, the flame height is close to 50mm. This increase in height is expected since nitrogen is a diluent and the flame needs additional height to entrain enough oxidizer to attain a stoichiometric mixture [47]. Figure 18 on the other hand, shows that with the addition of 3% and 11% water mist the flame heights dropped close to 30mm and 10mm, respectively. Figure 19 shows the IR images of the base case flame and flames with 7% nitrogen, 3% mist and 11% mist. By considering the location of the maximum temperature in each flame one observes that the flame height went up with the addition of nitrogen (a diluent) and went down with the addition of water mist. As the water droplets evaporate they form water vapor which is a diluent just like nitrogen and hence the dilution effect is expected to result in increase in flame height. The fact that the flame height goes down instead of going up with the addition of water mist suggests that some other important phenomenon may be taking place with the addition of mist. One could speculate that the following phenomena may be responsible. (I) The rapid cooling of the flame gases

as droplets evaporate very close to or within the flame sheet envelop may have Arrhenius effects on the combustion reactions. Since the flame is flickering the transport of droplets into the flame sheet envelope may have been enhanced. (ii) Based on Burke Schumann's theory, Roper [48] suggested that in a diffusion flame, unsteadiness would result in the lowering of flame height since flickering is known to enhance diffusion of fuel and oxidizer [49]. Indeed, if flickering also enhances entrainment, then it will be a desirable phenomenon for fire suppression.

4.4: Contributions from Oxygen Dilution, Sensible heat and Latent Heat in Water Mist Suppression of Flame temperature

The degree of suppression caused by a suppressant is defined in terms of the drop in temperature between two corresponding locations in the base case flame and in the flame with the suppressant. It may be unfair to compare two locations at the same distance above the burner since the flame height changes when a suppressant is added and the two locations may be dissimilar in terms of net heat release rate. For example, Figure 18 shows that 35mm above the burner the region around the center line of symmetry will be within the flame sheet envelope in the base and nitrogen cases but outside the envelope in the 3% and 11% mist cases. Therefore, for the purpose of this paper, the degree of suppression is defined in terms of the maximum flame temperature wherever it occurs. Figures 20 compares the degree of suppression in maximum flame temperature predicted from the analysis with the experimental data for nitrogen, steam and water mist. Degree of suppression is shown in terms of dimensionless temperature drop, where temperature drop is defined as the difference in the maximum flame temperature with suppressant and without suppressant. The Figure shows that the predicted suppression effect with nitrogen addition is in good agreement with the measured data. With steam, on the other hand, the theory appears to under predict the data. Recall that steam was produced by covering the co-flow air channel with a heated fine screen. Although the screen also heats up the co-flow air as the droplets evaporate, it is possible that within the 4cm length of the flame, the resulting mixture of steam and hot air could cool down below 373 K before it enters the high temperature zone of the thermal boundary layer. If this happens some of the steam will condense and a mixture that will include some fine water droplets will enter the flame. Thus, some latent heat effects will give rise to a higher suppression than would be measured if there was no condensation. The problem of steam condensation is expected to be more acute at higher mass fractions of steam in the co-flow air. The fact that the agreement between theory and data is worst 11% mass fraction of steam, seems to suggest that steam condensation probably took place in some of these tests. Although the power supply to the screen was increased at higher steam mass fractions, this probably did not superheat the steam enough. The analytic results and experimental data are in fairly good agreement in the water mist tests despite flame flickering. The agreement is better at higher mist mass fractions where the droplet mean diameters are in the range of 53 to 66μm.

Finally, the heat transfer coefficient, which was calculated from the base case in the analysis, may well be significantly higher with the addition of mist and steam because of the evaporation of water droplets outside the flame. This factor will contribute to the difference between the measured and predicted data since it will result in lower values of the predicted flame temperature than was observed, especially in the water mist and steam cases.

The magnitudes of the contributions from latent heat, heat capacity and oxygen dilution are shown more clearly in Figure 20. The difference between the mist data and the steam data is the effect of latent heat. The effect of higher heat capacity of steam is shown by the difference between the steam and nitrogen data, while the difference between the nitrogen data and the abscissa represents oxygen dilution effect. It can be observed that thermal cooling by latent heat absorption has the largest effect. Furthermore, the cooling effect from the higher heat capacity of steam is significant. Indeed, one can further deduce that the oxygen dilution effect is less than the gas phase cooling effects (sum of latent heat and higher heat capacity effects). For example, at the 11% mist mass fractions (66μm SMD) about 75% of the temperature drop will be due to the effects of thermal cooling. Although, the data show that the 53 to 66μm droplets have more of the effects of gas phase cooling, the 29μm droplet data suggest that smaller droplets may have more of the dilution effects. This may be so, since small droplets are more likely to evaporate outside the flame [28]. More data points at small droplet size will be needed to confirm this conclusion.

5. CONCLUDING REMARKS

This study has focused on the suppression of a small 2D methane diffusion flame by the addition of small quantities of mist, steam and nitrogen in the co-flowing air. The mist, steam and additional nitrogen mass fractions in the co-flow air range from 0.034 to 0.11. The measured droplet Sauter mean diameters are between 29μm and 66μm. A simple model of the flame predicted results which agree with the measured data. This study shows the effects of water mist on flame temperature and flame height. First, the suppression effect of water mist on flame temperature has three components, namely, effect of latent heat, higher heat capacity of water vapor (compared to air) and oxygen dilution. The present results show that all three effects are important in temperature suppression. Latent heat has the largest effect and the higher heat capacity effect is significant. These two effects constitute gas phase cooling. The results show that the contribution from gas phase cooling mechanism is slightly larger than that of oxygen dilution effect, especially when the droplet Sauter mean diameters are in the range of 60μm. Finally, the introduction of water mist in the flame makes the flame flicker and the flame height to go down. We suspect that flickering enhances the diffusion of fuel and oxidizer and this results in shorter flames. A more careful investigation is required to verify this speculation.

6.0 ACKNOWLEDGMENTS

The assistance of Dr. John Hoover, Roger Brown, Glenn Salmon and Howard Burchell in this work is appreciated. We thank the Optical Sciences division for loaning us the equipment for IR measurements. The work described in this paper was performed by the Chemistry Division of the Materials Science and Component Technology Directorate, Naval Research Laboratory. The work was funded by the office of Naval Research, Code 334, under the Damage Control Task of the FY97 BA2 Surface Ship Hull, Mechanical, and Electrical Technology Program (PE0602121N)

7.0 REFERENCES

1. Butz, J. R., and Carey, R., "Application of fine water mist to fire suppression," Proceedings of the Halon Alternative Technical Conference, Albuquerque, NM, May 1992.

2 Wighus, R., "Fine water spray system - Extinguishing tests in medium and full scale Turbine Hood," SINTEF NBL, Norwegian Fire Research Laboratory 1993.

3 Papavergos, P.G., "Fine water sprays for fire protection" Proceedings of the Halon Alternative Technical Conference, Albuquerque, NM, May 1991.

4 Hill, R. G., Sarkos, C.P., and Marker, T.R "Development and evaluation of an on-board aircraft water spray system for postcrash fire protection" SAE Technical Paper 912224, Aerospace Technology Conference and Exposition, Long Beach, California, September 23-26 1991.

5 Hill, R.G, Marker , T.R, and Sarkos, C.P., "Evaluation of an On-Board water spray fire suppression system in aircraft," Presented at the water mist fire suppression workshop, National Institute of Standards and Technology, Gaithersburg, Maryland March 1 1988.

6 Marker, T.R., On-Board cabin water spray system under various discharge configurations," Federal Aviation Administration, Report DOT/FAA/CT-TN91/42, October 1991.

7 Whitfield, R.T., Whitfield, Q.A., and Steel, J., " Aircraft cabin fire suppression by means of an interior water spray system", Civil Aviation Authority, CAA paper 88014, July 1988.

8. Back, G.G, DiNenno, P.J., Leonard, J.T., and Darwin, R.L "Full Scale tests of water mist fire suppression systems for Navy shipboard machinery space: Phase I - Unobstructed spaces" NRL Memorandum Report NRL/MR/6180-96-7830. March 1996.

9. Mawhinney, J.R. Engineering criteria for water mist fire suppression systems *Proceedings of the Water mist fire suppression workshop* (Notarianni, K.A. and Jason, N.H. eds.), NISTIR 5207 March 1993, pp.37-73.

10. Mawhinney, J.R. Design of water mist fire suppression systems for shipboard Enclosures *Proceedings of Water Mist instead of Halon? - an International Conference on water mist fire suppression systems,* Boras, Sweden November 1993

11. Gameiro, V. M. "Fine water spray fire suppression alternative to halon 1301 in machinery spaces", *Proceedings of the International CFC and Halon Alternative Conference,* Washington D.C October 20-22, 1993.

12 Bill, R.G., Hansen, R.L.,and Richards, K., "Fine spray protection of shipboard engine room" Proceedings of the NIST Annual Fire Conference, Gaithersburg, Maryland October 28-31, 1996, p.19

13 Arvidson, M., "Efficiency of different water mist systems in a ship cabin" *Proceedings of International Conference on Water Mist Fire suppression systems -- Water Mist Instead of Halon?*, Boras, Sweden November 4-5 1993.

14. Tatem, P.A., Beyler, C.L., DiNenno, P.J., Budnick, E. K., Back, G.G. and Younis, S.E "A review of water mist technology for fire suppression" NRL Memorandum Report No.NRL/MR/6180--94-7624 , Naval Research Laboratory, Washington D.C 1994

15 Rasbash, D.J., Rogowski, Z.W., and Stark, G.W.V. " Mechanism of extinction of liquid fires with water sprays" *Combustion and Flame*, 4 :223 (1960).

16. Rasbash, D.J., and Rogowski, Z.W "Extinction of fires in liquids by cooling with water sprays," *Combustion and Flame*, **1** :4, (1957).

17 Rasbash, D.J. "The Extinction of fires by water sprays," *Fire Research Abstracts and Reviews*, **4** (1&2): 28, (1962).

18 Braidech, M.M, Neale, J.A., Matson, A.F. and Dufour, R.E., " The mechanism of Extinguishment of fire by finely divided water", Underwriters Laboratories Inc. for the National Board of fire Underwriters, N.Y., p. 73 1955.

19 Jackman, L.; Glockling, J.L; and Nolan P.F "Water Sprays: Characteristics and effectiveness" *Proceedings of the Halon alternative technical Conference*, Albuquerque N.M May 11-13 p.263, 1993.

20 Rogers, G.F and Mayhew, Y.R; "Thermodynamic and Transport Properties of Fluids". Basil Blackwell, Oxford 1981.

21. Log, T. "Radiant heat attenuation in fine water Spray" *Proceedings of INTERFLAM*, Cambridge UK March 26-28, p.425, 1996.

22 Coppalle, A; Nedelka, D. And Bauer, B. " Fire Protection: Fire Curtains" *Fire Safety Journal* **20** : 241, (1993).

23 Thomas, P.H.; " Absorption and scattering of radiation by water sprays of large droplets" *British J. of Appl. Phy.* **3:**385, (1952).

24 Mawhinney, J.R. "Characteristics of water mists for fire suppression in enclosures" *Proceedings of Halon Alternatives Technical working conference* Albuquerque, New Mexico May 11-13 1993.

25 Hanauska, C.P and Back, G.G, "Halon alternative Fire protection systems, An over view of water mist fire suppression system technology", Hughes Associate Inc. Columbia , MD. 1993

26 Yang J. Private Communication

27 Seshadri, K "Structure and extinction of laminar diffusion flame above condensed fuels with water and nitrogen" *Combustion and Flame* **33**:197(1978).

28 Lentati, A.M and Chelliah, H.K; "The dynamics of water droplets in a counterflow field and its effects on flame extinction" Fall Technical Meeting, The Eastern States section of the Combustion Institute, Hilton Head, SC Dec. 9-11 1996.

29 Li, S.C; Libby, P.A. and Williams, F.A; "Spray Impingement on a hot surface in reacting stagnation flows" *AIAA Journal*, **33** (6) :1046 (1995).

30 McCaffrey, B.J; "Jet diffusion flame suppression using water spray -- An interim Report" *Combustion Science and Technology* **40** :107 (1984).

31 Ndubizu, C.C; Motevalli, V and Tatem P.A.; Study of the suppression mechanisms of small flames by water mist." Fall Technical Meeting, The Eastern States section of the Combustion Institute, Worcester, MA. Oct. 16-18 1995.

32 Prasad, K.; Li, C.; Kailasanath, K.; Ndubizu, C.; Ananth, R. And Tatem, P. "Numerical Modeling of water mist suppression of methane-air diffusion flames" *Combustion Science and Technology.* In press.

33 Prasad, K.; Li, C.; Kailasanath, K.; Ndubizu, C.; Ananth, R. And Tatem, P. "Numerical Modeling of fire suppression using water mist. 1. Gaseous Methane - Air Diffusion Flames" NRL Memo Report NRL/MR/6410-97-

34 Wolfhard H.G. and Parker W.G.; " A new technique for the spectroscopic examination of flames at normal pressures" *Proc. Phys. Soc.* (London) **A62:**722 (1949).

35 Ndubizu, C.C; Ananth, R; Tatem, P.A; and Motevalli V; "On water mist fire suppression mechanisms in a gaseous diffusion flame" *Journal of Fire Safety.* In press.

36 Reeds K. (Delavan Inc.) Private communication

37 The Temperature Handbook, Vol. 29; Omega Engineering Inc. 1995. pp. Z159.

38. Gordon S., and McBride, B.J., Computer Program for Calculation of Complex Chemical Equilibrium Compositions and Applications. NASA Reference Publication 1311, Lewis Research Center Cleveland, OH (NASA, Washington, DC October 1994).

39. Beyler C. A unified model of fire suppression *J. of Fire Prot. Engr.* **4** (1): 5 (1992).

40. Teweson, A. Generation of heat and chemical compounds in fires. In *SFPE Handbook of Fire Protection Engineering*, DiNenno P.J et. al. (Editors); National Fire Protection Association, Quincy MA. (1995) pp. **3**-112

41. Ewing C.T ; Hughes, J.T ; and Carhart, H. W.; The Extinction of hydrocarbon flames based on the heat -absorption processes which occur in them. *Fire and Materials*, **8** (3):148 (1984).

42 Smyth, K.C., Miller, J.H.,Dorfman, R.C.,Mallard, W.G.,and Santoro,.R.J. " Soot Inception in a Methane/ Air Diffusion Flame as Characterized by Detailed Species Profile", *Combustion and Flame* **62**:157 (1985)

43 Mitchell, R.E; Sarofim, A.F and Clomburg L.A; "Experimental and numerical investigation of confined laminar diffusion flames" *Combustion and flame* **37:**227 (1980).

44 McEnally C.S., and Pfefferle L.D Aromatic and Linear Hydrocarbon Concentration Measurements in a non-premixed Flame, *Proceedings of the Fall Technical Meeting, The Eastern States Section of the Combustion Institute.* p. 249-252 Worcester MA Oct. 1995

45 Glassman, I. *Combustion.* Academic Press, Inc., Orlando Fl. 1987 p.25.

46 Atreya, A; Crompton, T; and Suh, J; An Experimental and Theoretical Study of Mechanisms of fire suppression by water. *NIST annual Conference for Fire Research* Oct. 17-20 1994 NISTIR 5499, pp. 67

47 Burke, S. P and Schumann, T.E.W. " Diffusion Flames". *Ind. Eng. Chem.* **20**:2 (1928).

48 Roper, F.G; Smith, C; and Cunningham, A.C. "The Prediction of Laminar jet diffusion flame sizes: Part II, Experimental Verification". *Combustion and Flame* **29:**227 (1977).

49 Goudie, G.O., Mixing and Combustion of gas Jets . Ph.D Thesis University of Glasgow, 1967.

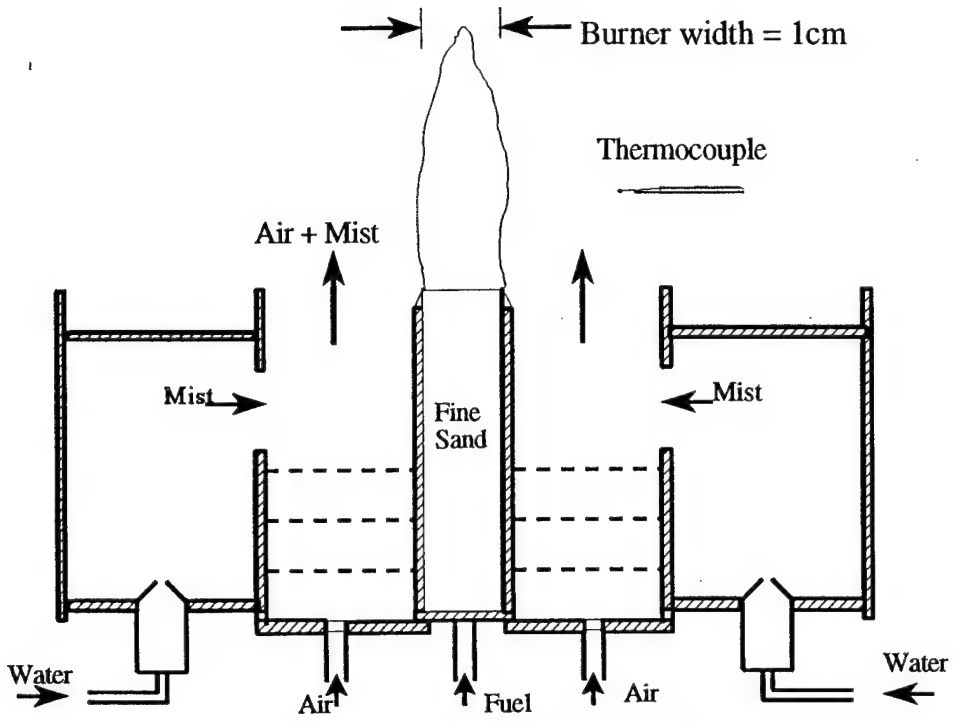

Figure 1a: The Modified Wolfhard - Parker burner

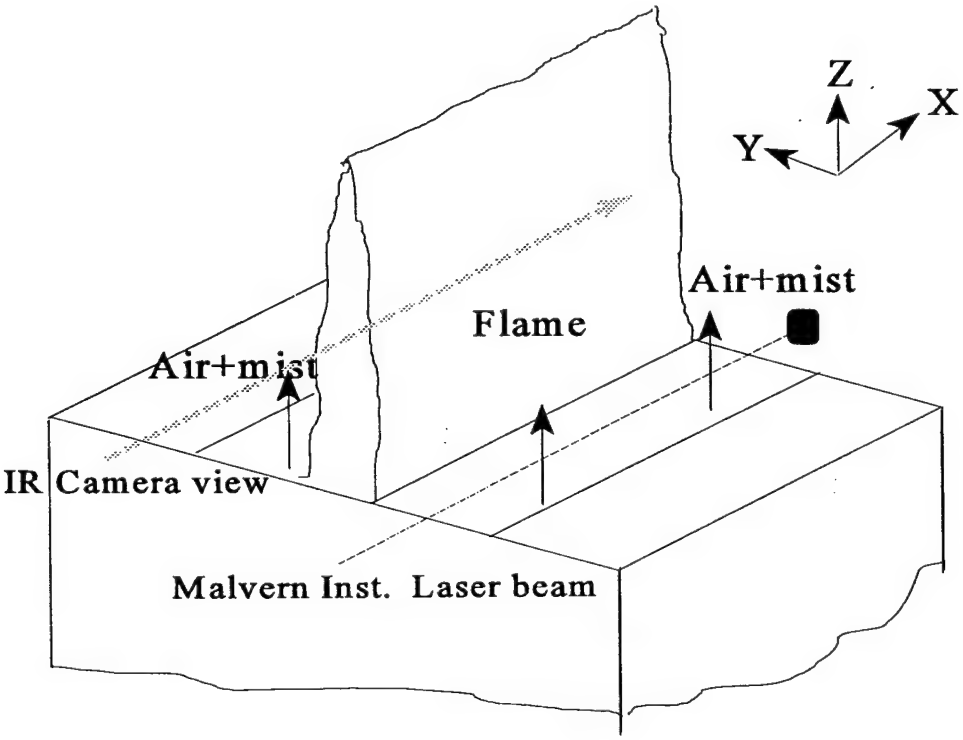

Figure 1b: The 2D Flame

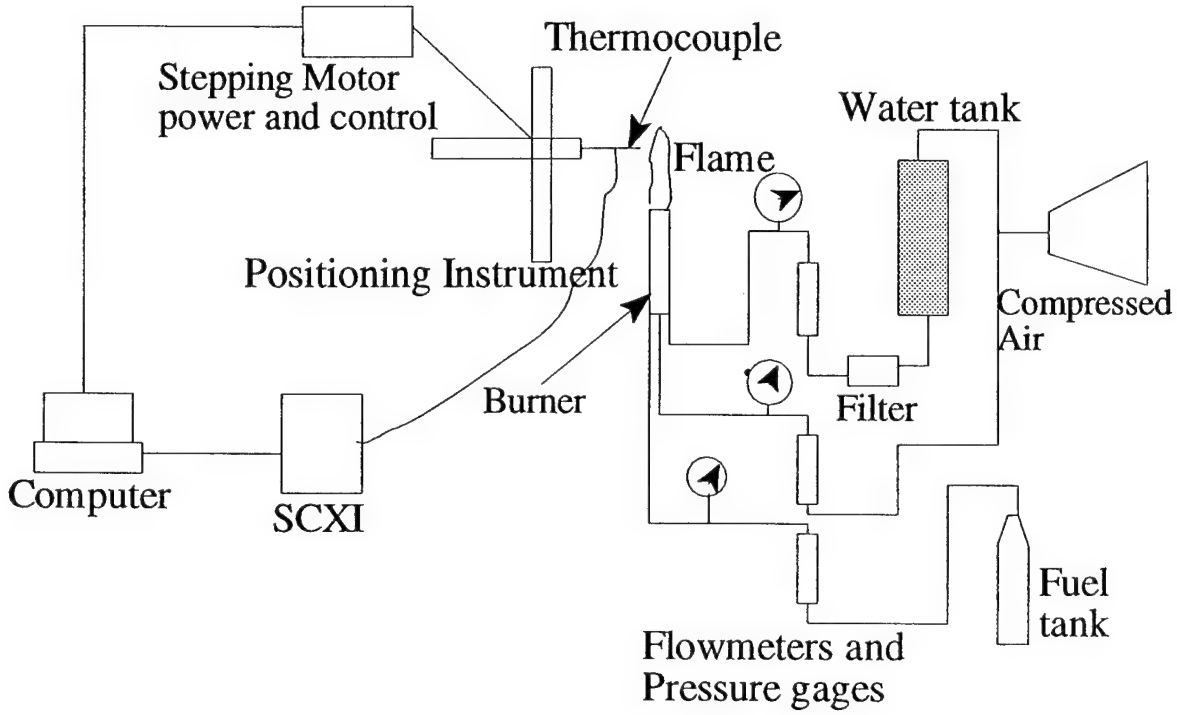

Figure 2: Schematic of the Experimental setup.

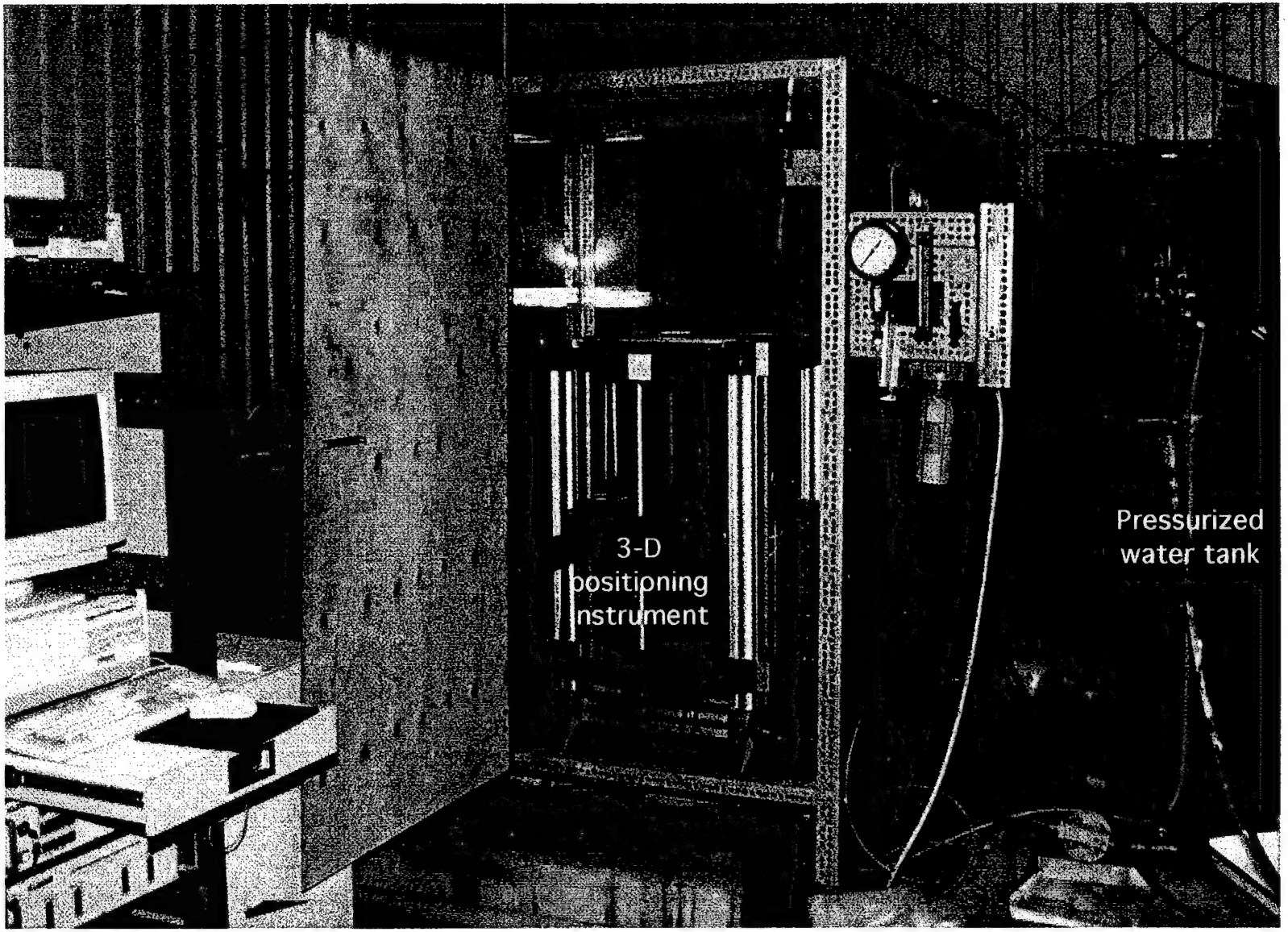

Figure 3: A Picture of the Experimental Setup

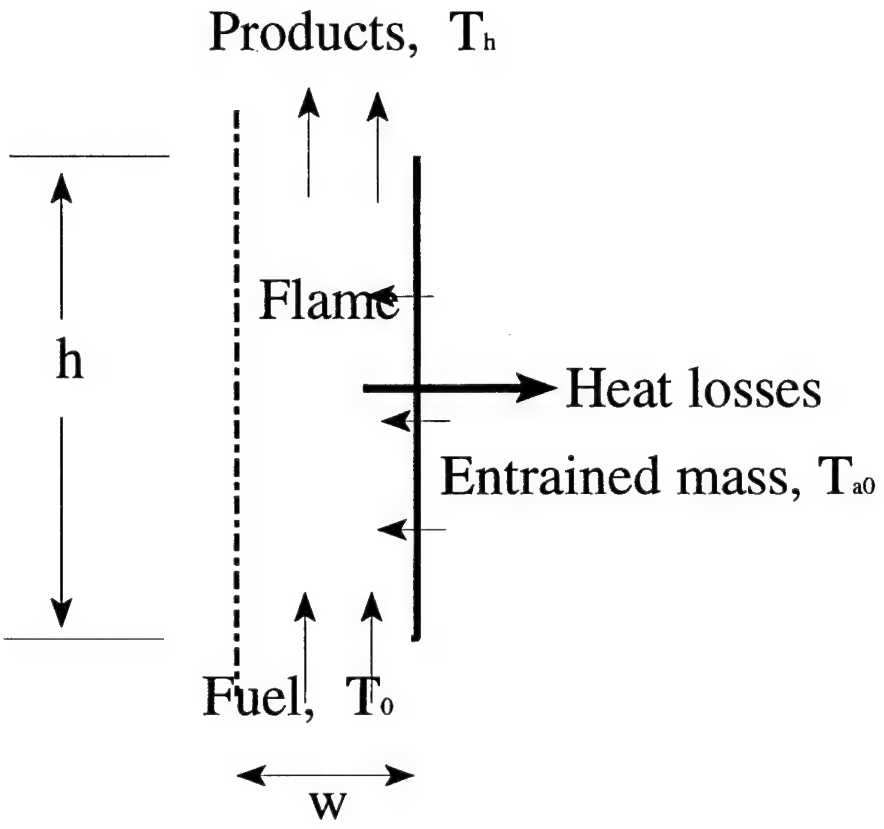

Figure 4:Schematic model of the flame showing flow and heat transfer parameters

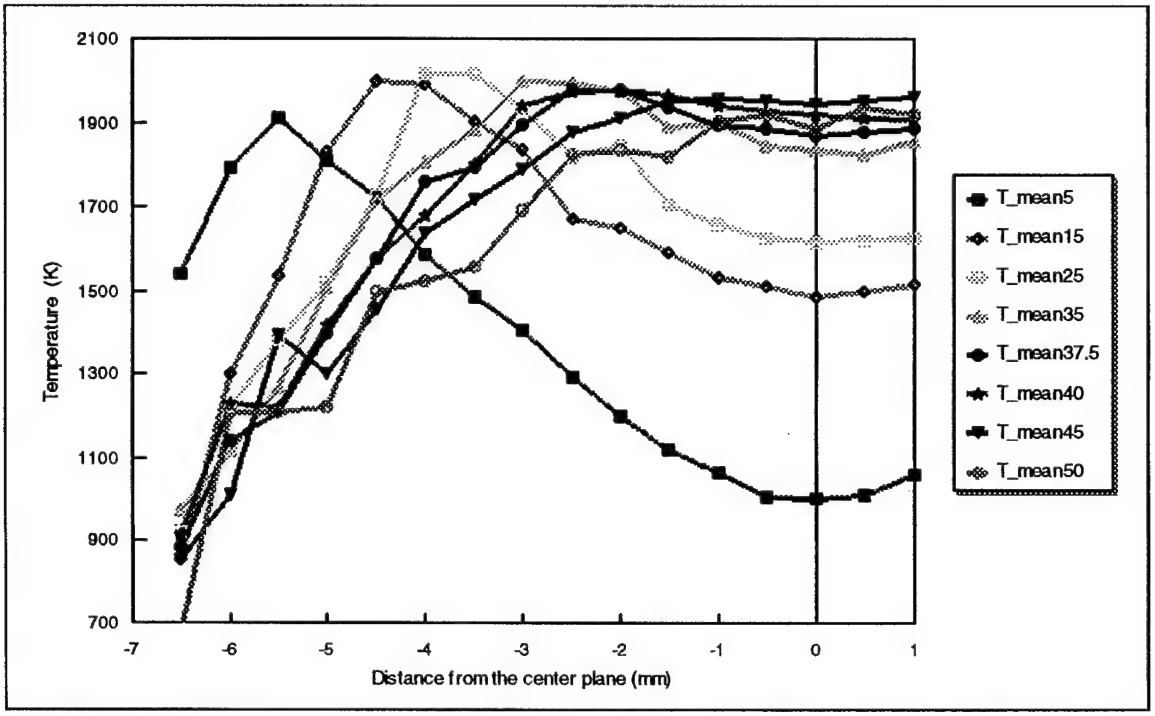

Figure 5: Temperature Profile across unsuppressed Methane-air diffusion flame (base case) at various heights above the burner.

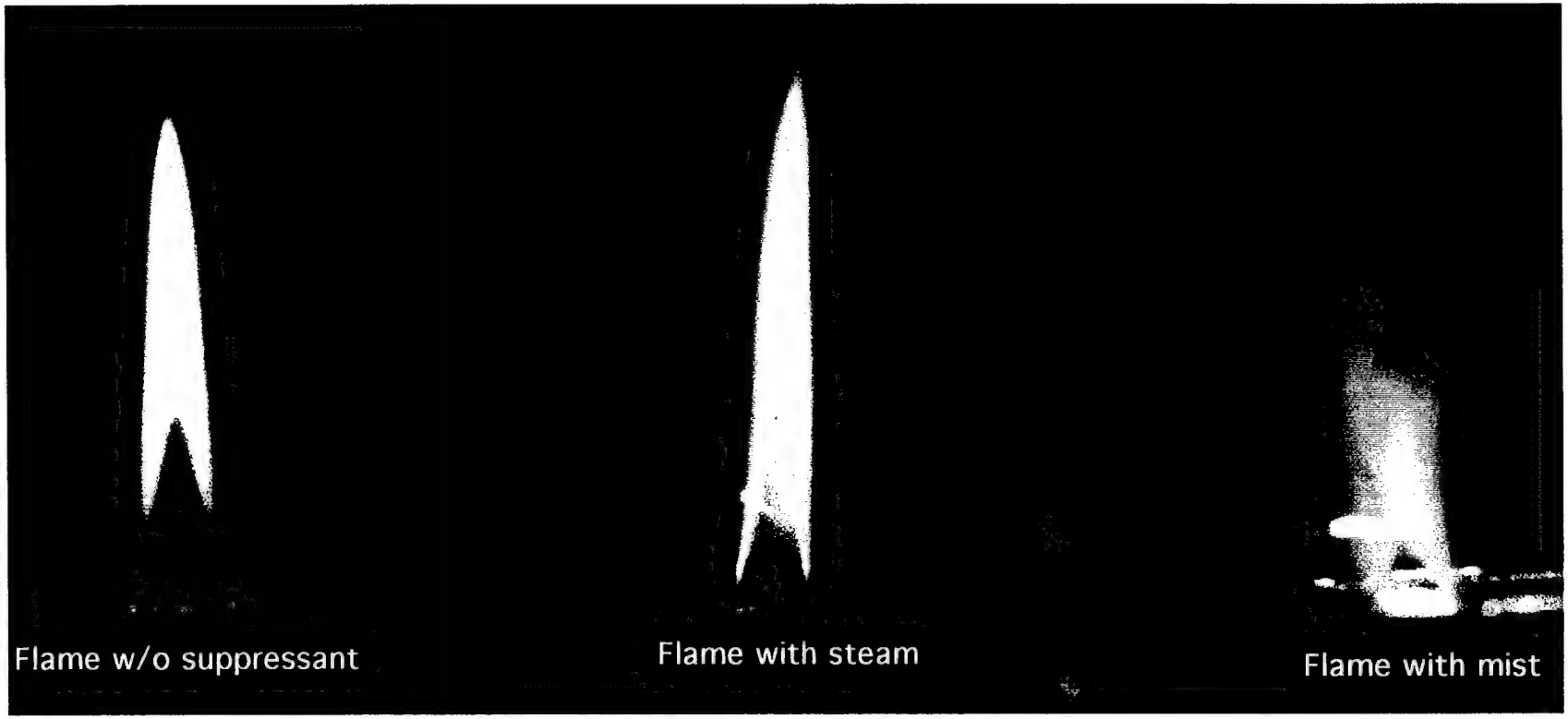

Figure 6: Picture of the flame without suppressant, with steam and with water mist

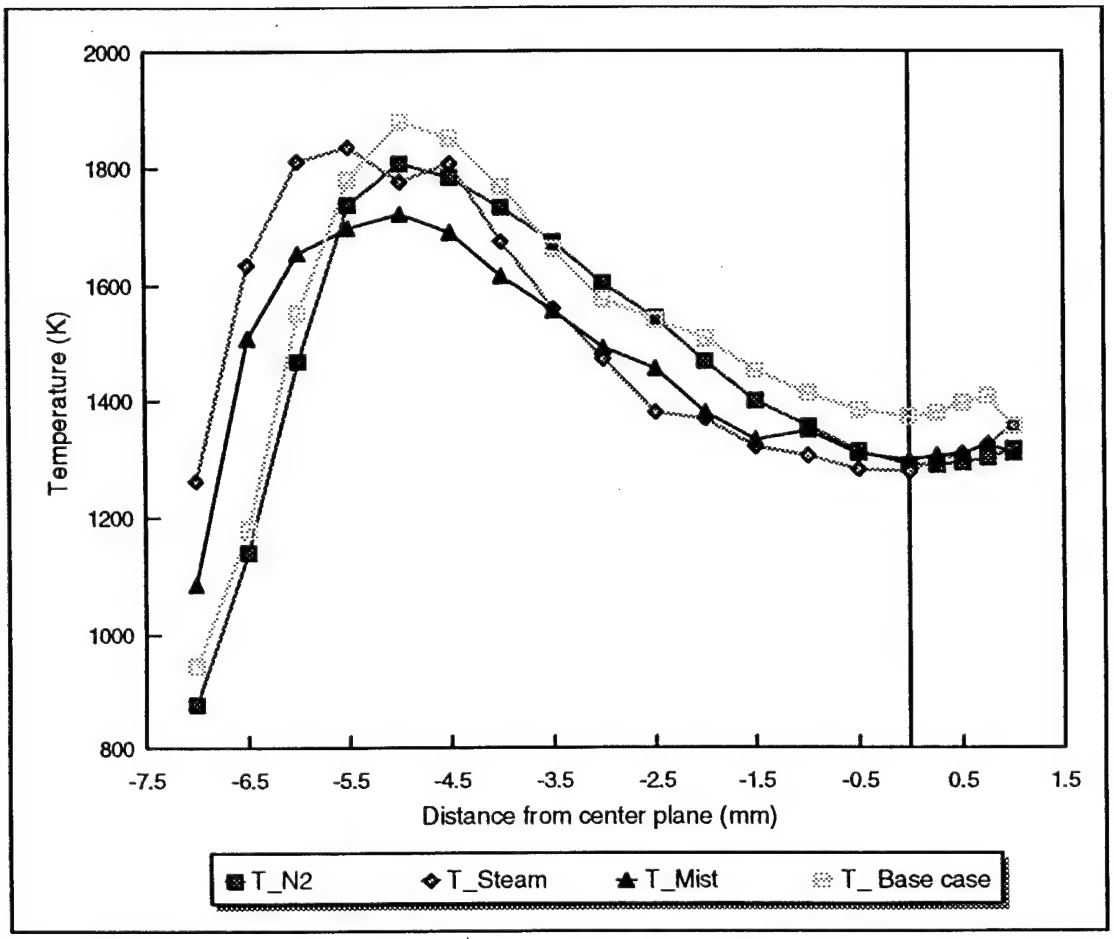

Figure 7: Temperature Profile 10mm above the burner for methane diffusion flame with Nitrogen, Mist and steam addition. Mass fraction of suppressant in air = 0.034

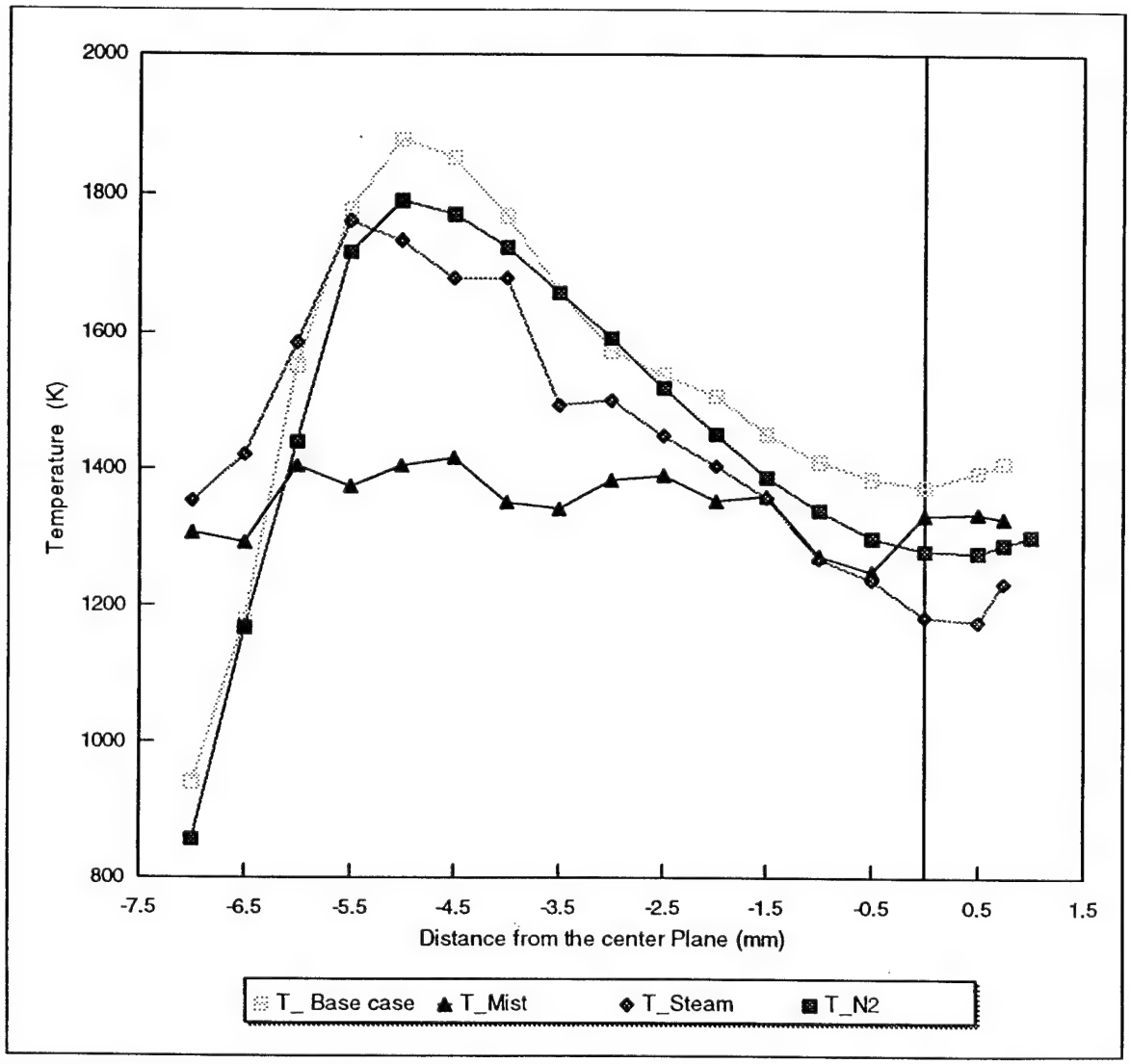

Figure 8: Temperature profile 10mm above the burner for methane diffusion flame With nitrogen, mist, and steam addition. Mas fraction of suppressant in Air = 0.34

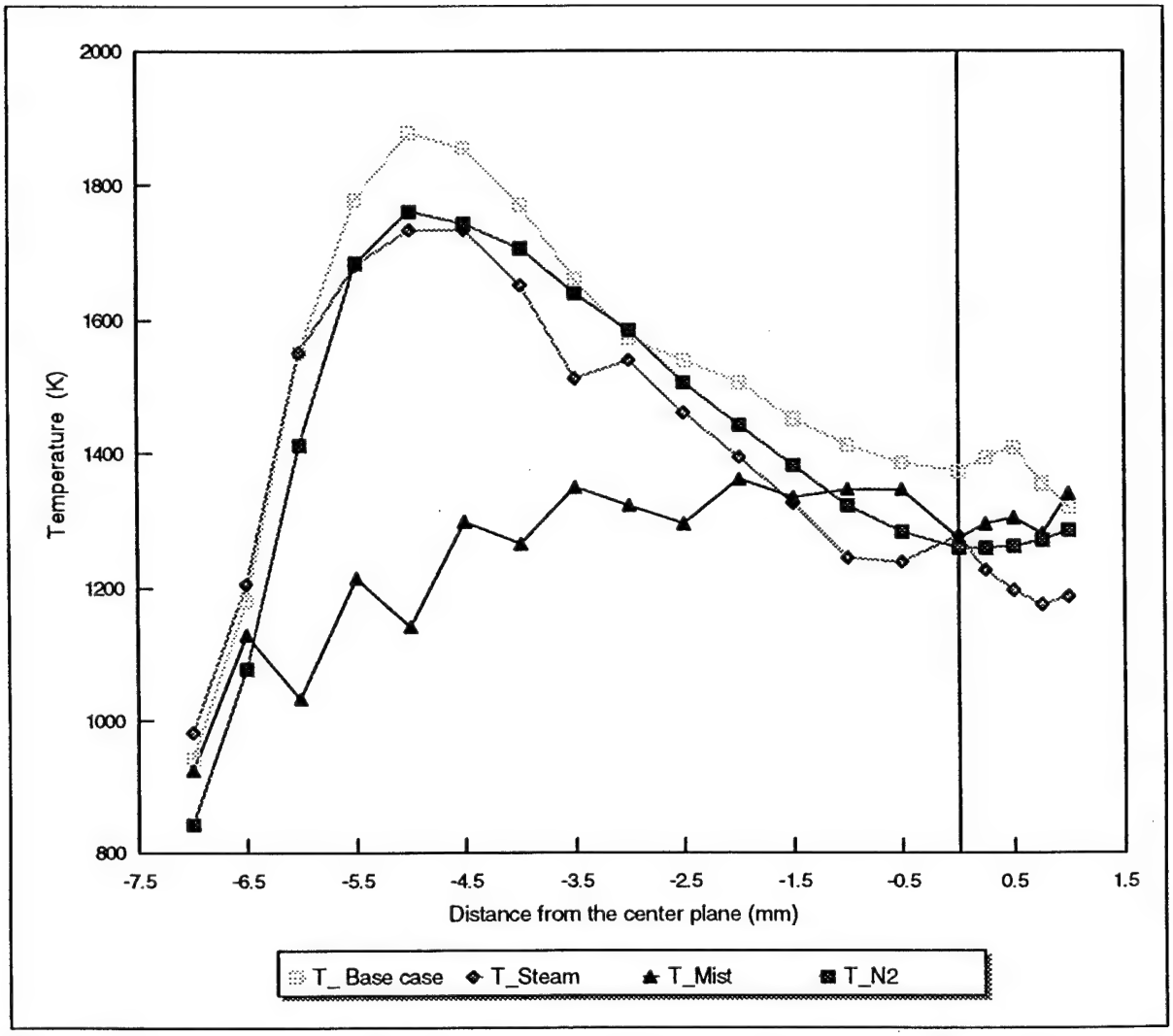

Figure 9: Temperature profile 10 mm above the burner for methane diffusion flame with nitrogen, mist and steam addition. Mass fraction of suppressant in air =0.07

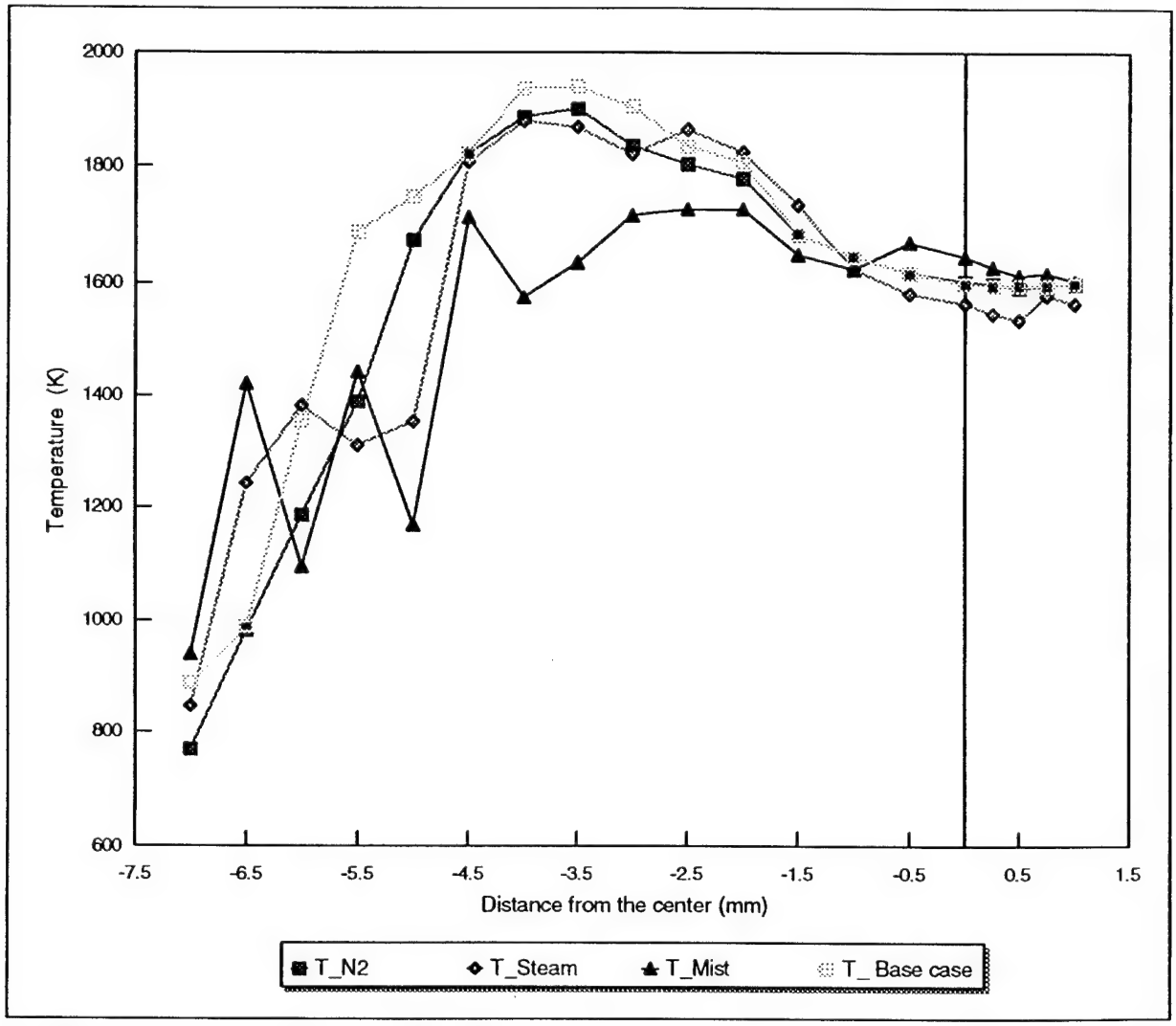

Figure 10 Temperature profile 30 mm above the burner for methane diffusion flame With nitrogen, mist and steam addition. Mass fraction of suppressant in air = 0.034

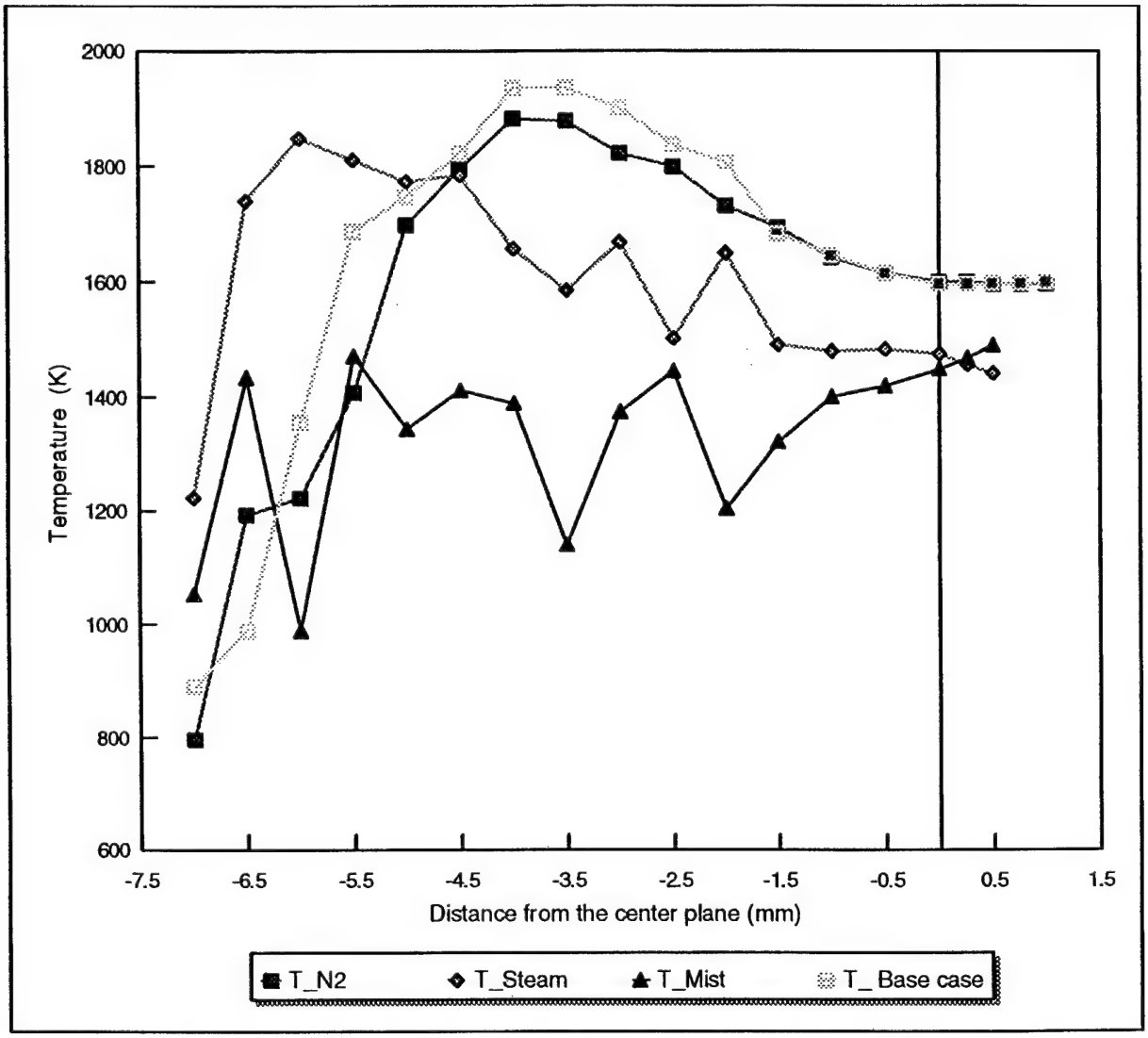

Figure 11 : Temperature Profile 30mm above the burner for methane diffusion flame with Nitrogen, Mist and steam addition. Mass fraction of suppressant in air = 0.05

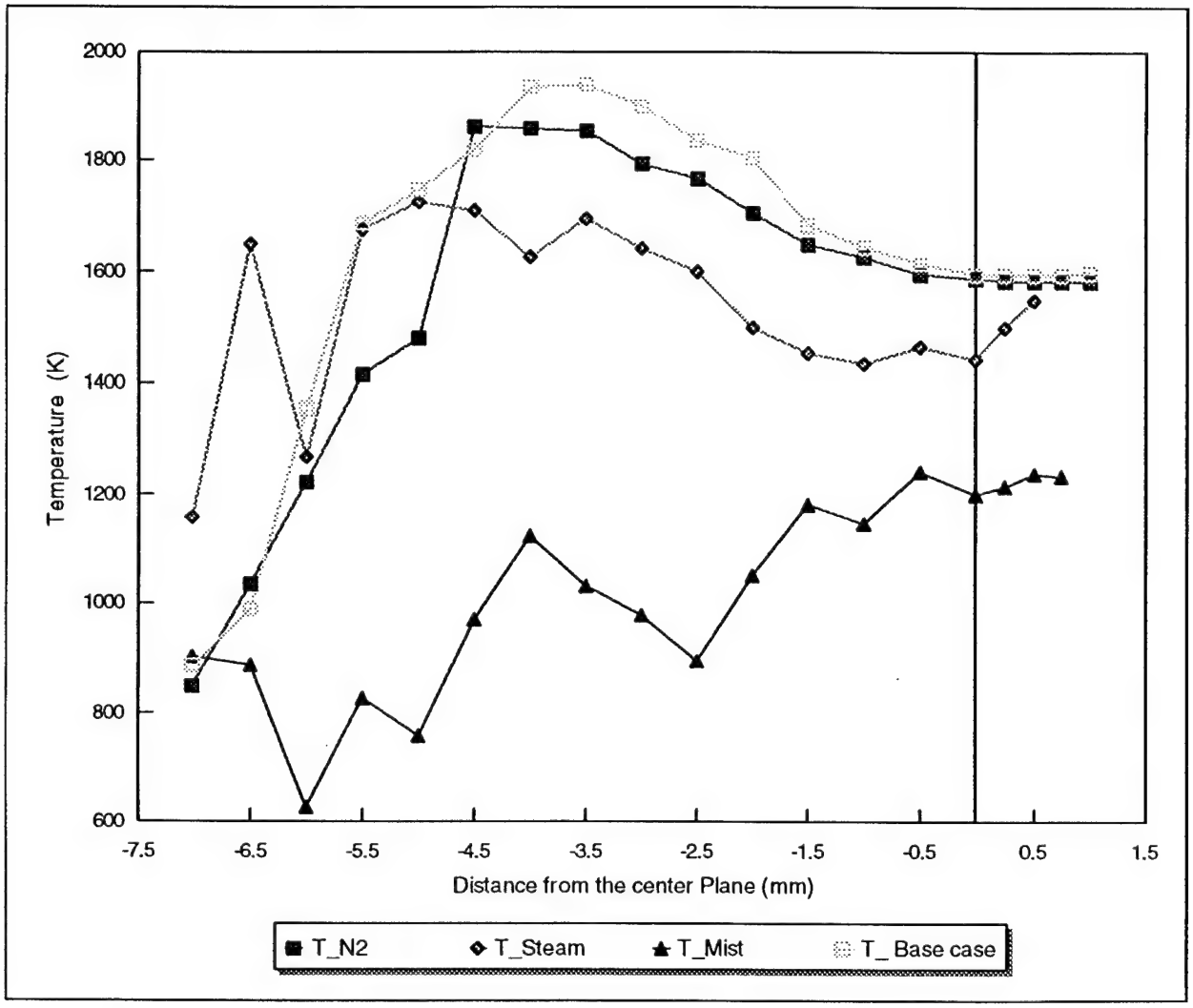

Figure 12: Temperature Profile 30mm above the burner for methane diffusion flame with Nitrogen, Mist and steam addition. Mass fraction of suppressant in air = 0.07

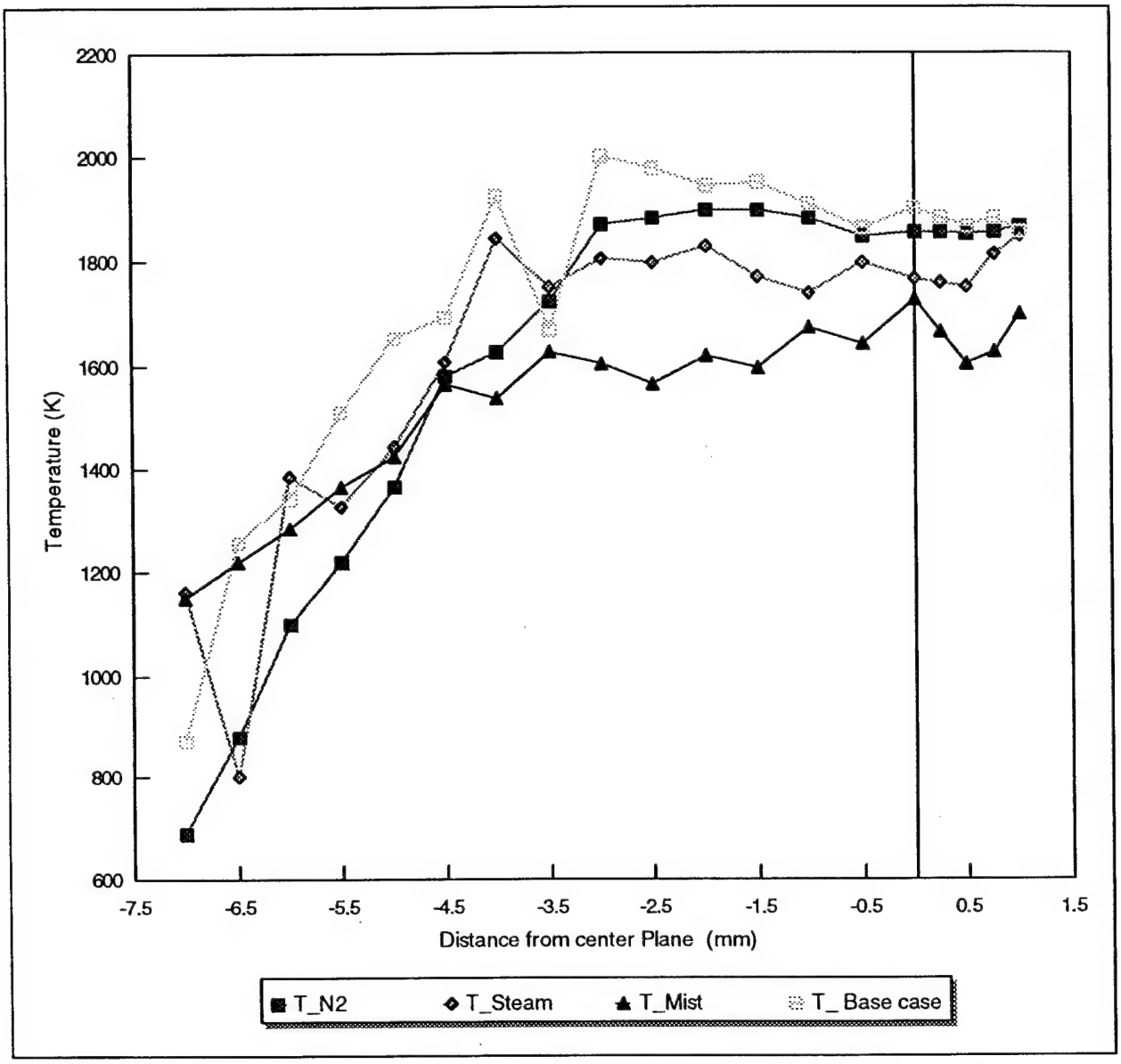

Figure 13: Temperature Profile 45mm above the burner for methane diffusion flame with Nitrogen, Mist and steam addition. Mass fraction of suppressant in air = 0.034

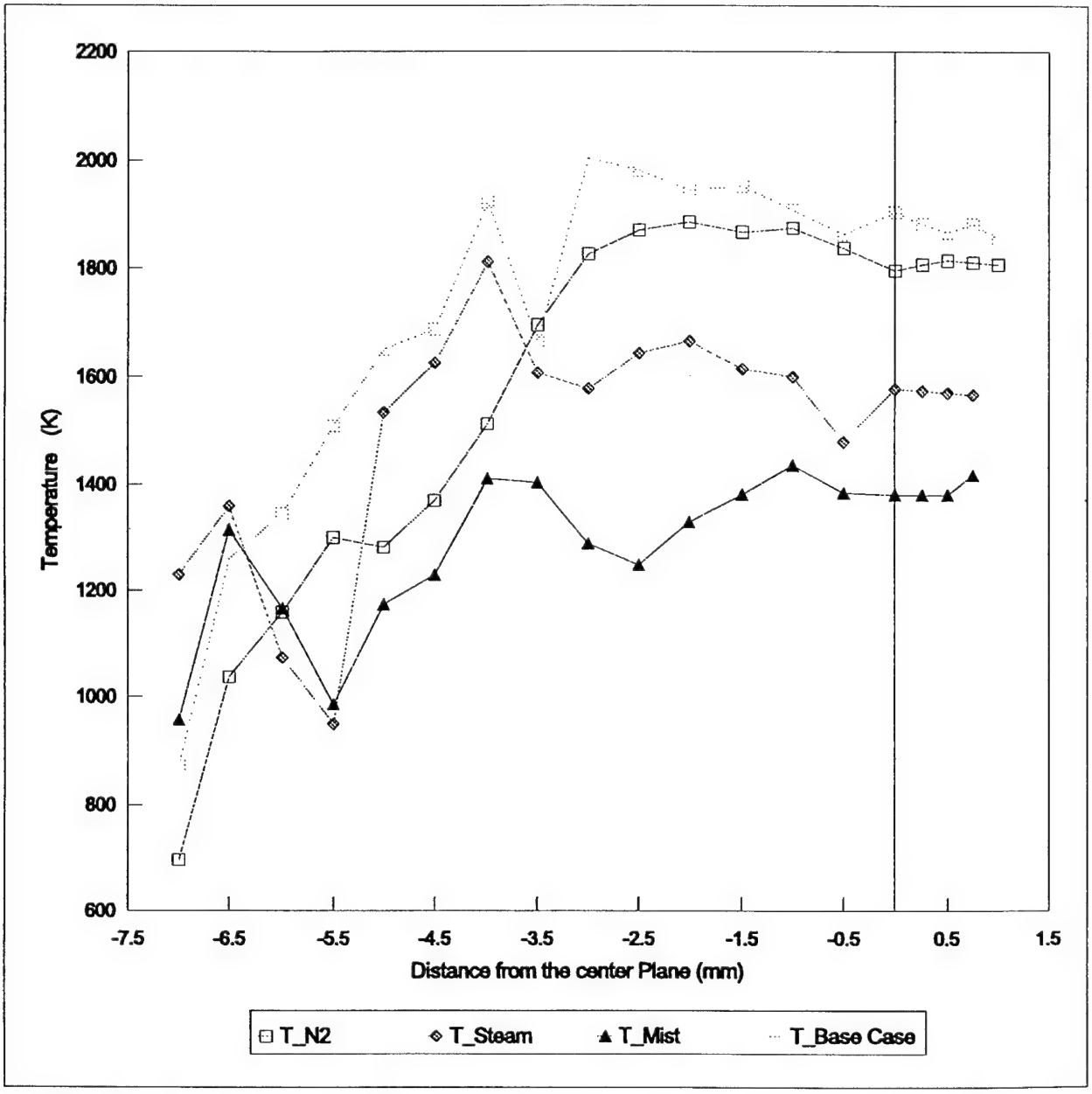

Figure 14: Temperature profile 45 mm above the burner for methane diffusion flame With nitrogen, mist and steam addition. Mass fraction of suppressant in Air = 0.05

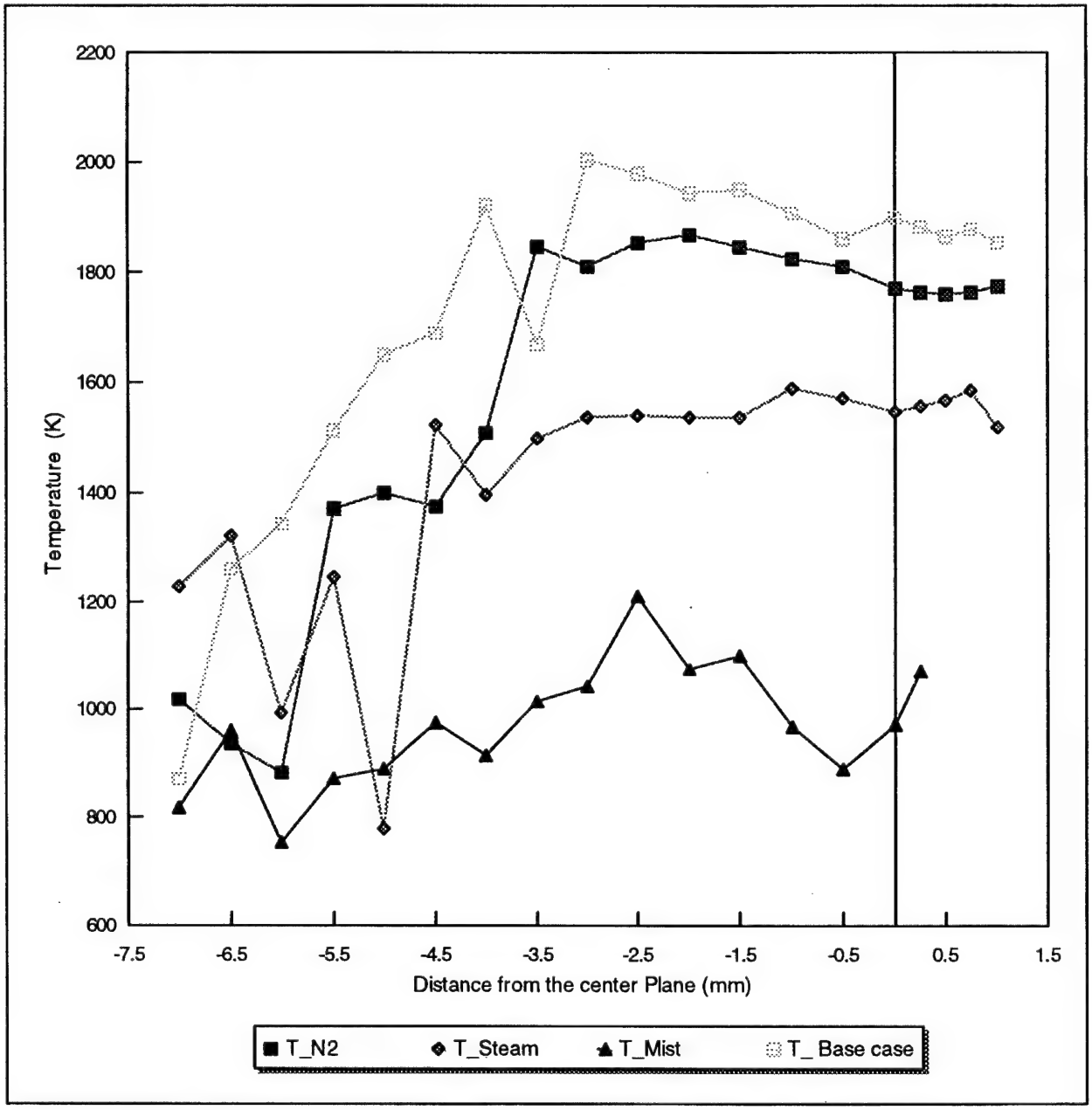

Figure 15: Temperature Profile 45mm above the burner for methane diffusion flame with Nitrogen, Mist and steam addition. Mass fraction of suppressant in air = 0.07

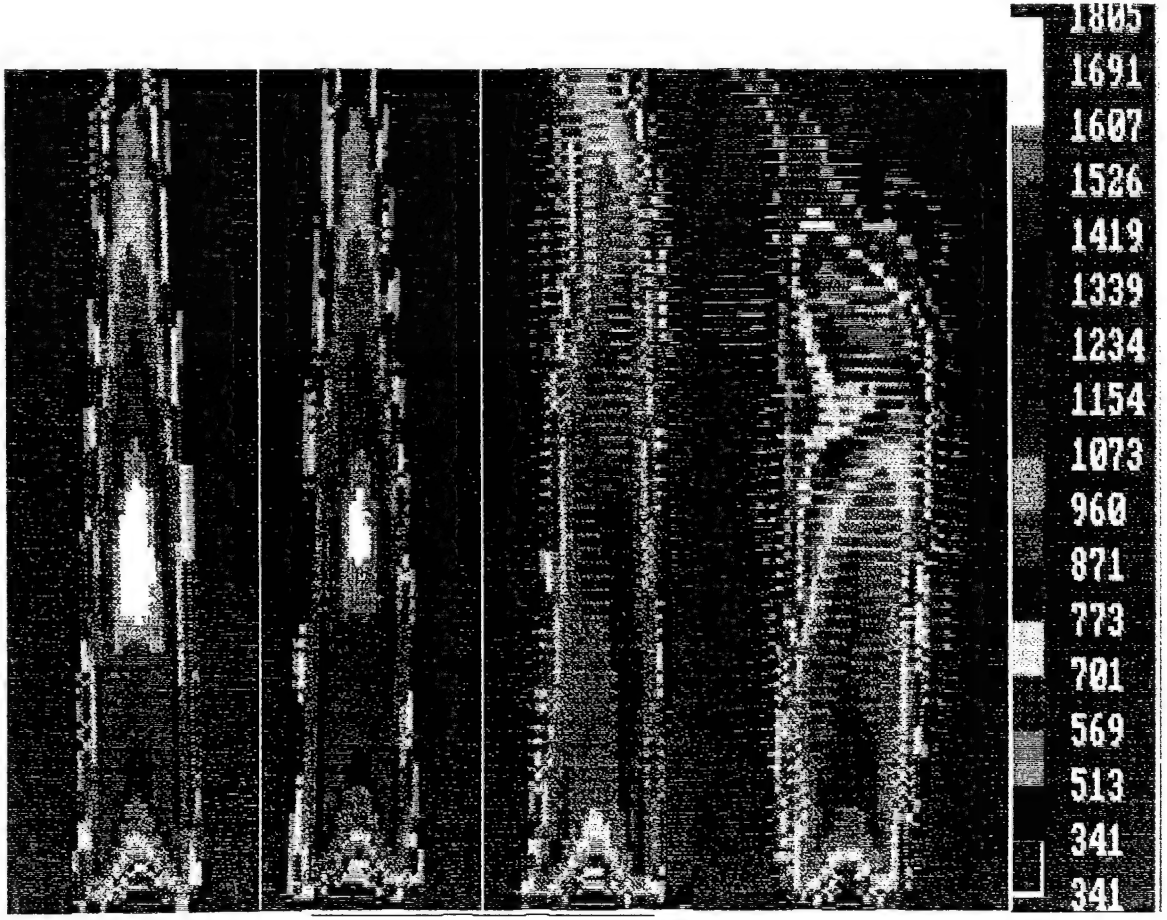

Figure 16: Infrared Images of the (a) base case flame, (b) flame with 3% N2, (c) flame with 3% steam, and (d) flame with 3% water mist

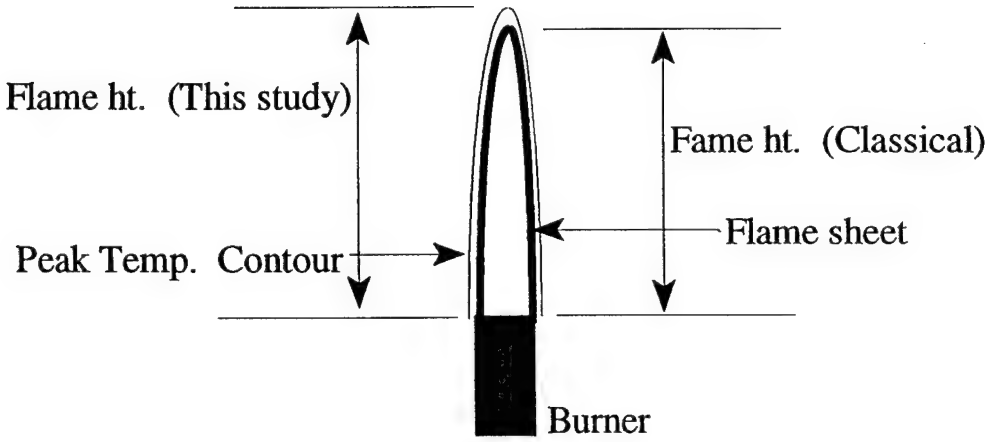

Figure 17: Schematic of the 2D flame to illustrate the definition of flame height in this study

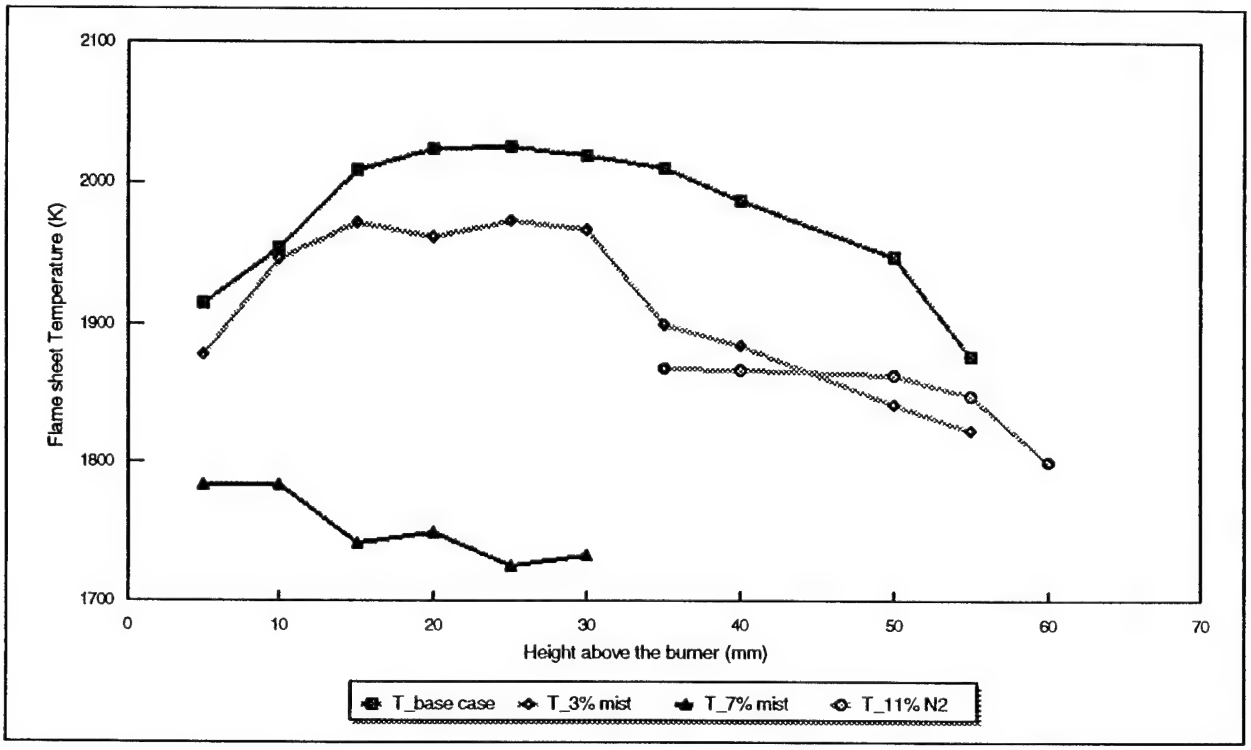

Figure 18: Flame peak temperatures at various heights, for the flames with no suppressant, 3% water mist, 7% water mist and 11% nitrogen in the co-flow air.

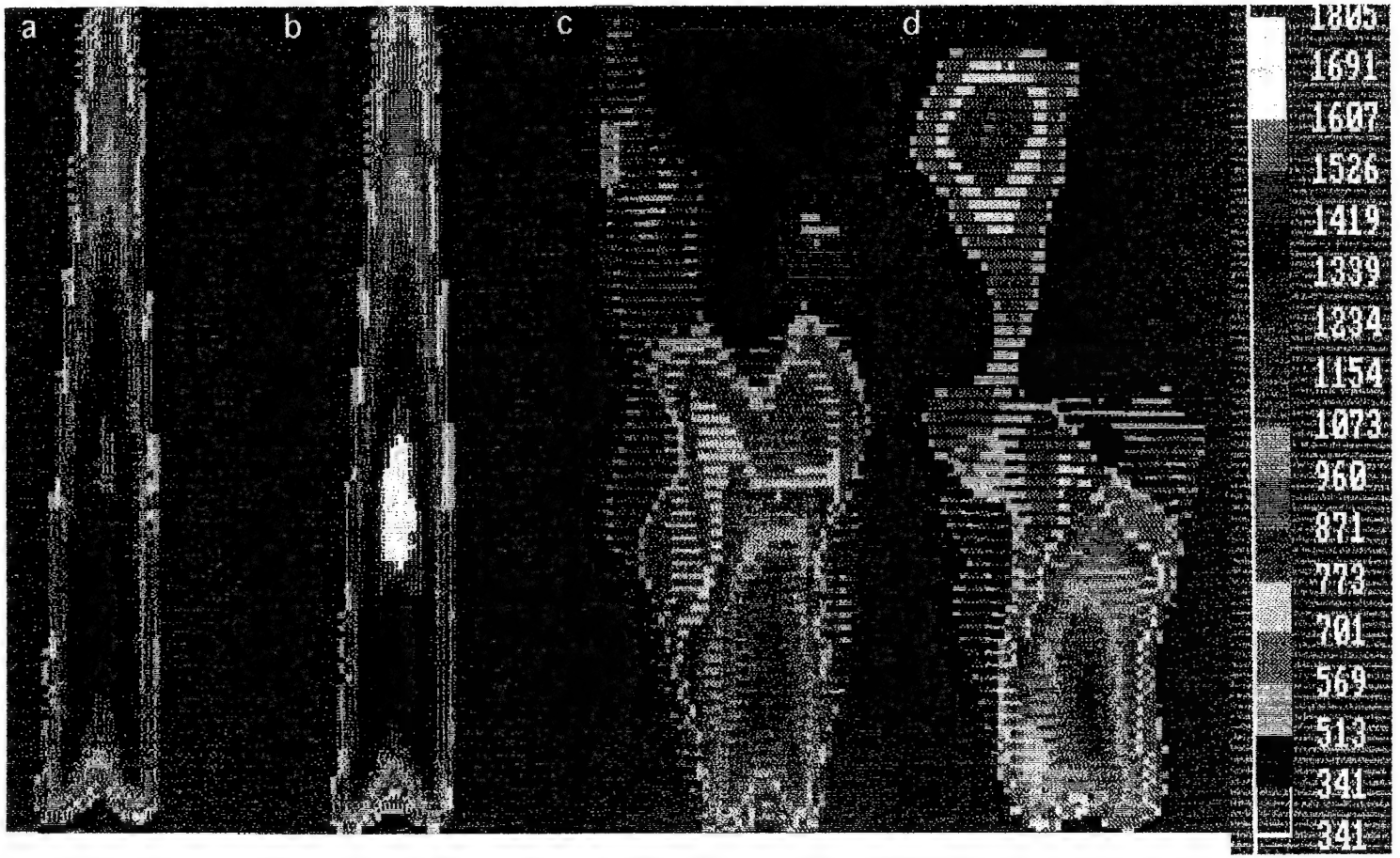

Figure 19: Infrared images of the flame with (a) 7% N2 (b) no suppressant, (c) 3% mist and (d) 11% mist

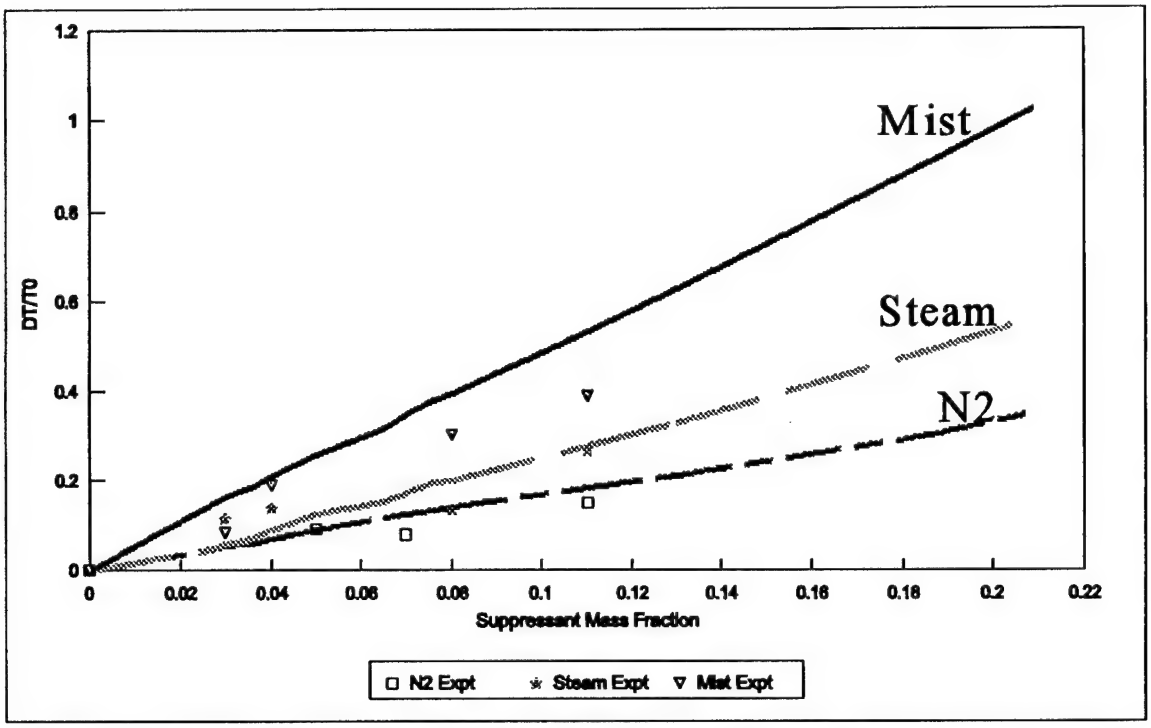

Figure 20: Degree of suppression at various concentrations of nitrogen, steam and water mist (Theory and Experiments)

TABLE 1 : Characterization of the mist leaving the oxidizer channel. Average air velocity = 18.1cm/s

Nozzle Type	Water Pressure (KPa.)	Mist flow rate leaving both channels (cc/min)	Measured droplet Sauter mean diameter (μm)	Mass fraction of mist in the co-flow
WDB 0.5-60°	482.6 (75 Psi.)	2.2 ±0.3	29.0 ±1.8	0.034 ±.0048
WDB 0.75-60°	482.6	2.5 ±0.1	56.1 ± 1.6	0.039 ± .0016
WDB 1.0-60°	482.6	3.3 ± 0.2	53.9 ± 1.2	0.050 ± .0032
WDB 1.5-60°	482.6	4.7 ± 0.2	65.8 ± 0.2	0.70 ± .0032

TABLE 2: Comparison of the measured and predicted maximum flame temperatures at various levels of Nitrogen Dilution.

Mass fraction of (additional) Nitrogen in the air	Net Mass fraction of oxygen in the air	Measured Maximum Temperature (K)	Predicted Maximum Temperature (K)	Predicted adiabatic Flame Temperature (K)- Theory	Adiabatic Flame Temperature (K) - NASA
0.0 (Base case)	.233	1946 (+or- 25)	1946*	2358	2250
0.065	.218	1875	1873	2249	2179
0.13	.203	1792	1814	2138	2101
0.186	.19	1742	1757	2040	2027
0.209	.184	1722	1727	1998	1994

* h_c was used as a fitting parameter for the base case. This same value of h_c was used for all the cases with a suppressant.

APPENDIX

Water mist droplet size distributions for tests with 3%, 5% and 11% mist

APPENDIX

The droplet size distribution curves obtained with the Malvern Instrument are shown in figures A.1 to A.3. The data were measured as the droplets leave the oxidizer channel (see figure 1b). Figure A.1 shows the distribution curve for tests when the mist mass fraction is 3% and the Sauter mean diameter is 29μm. The distribution shows that majority of the droplets have diameters between 25μm and 60μm and that up to 90% of the droplets have diameters below 100μm. For the mist mass fractions of 5% and 11%, the distributions are narrower. The Sauter mean diameters are 54μm and 66μm, respectively. In each case, 65% of the droplets have diameters less than 100μm.

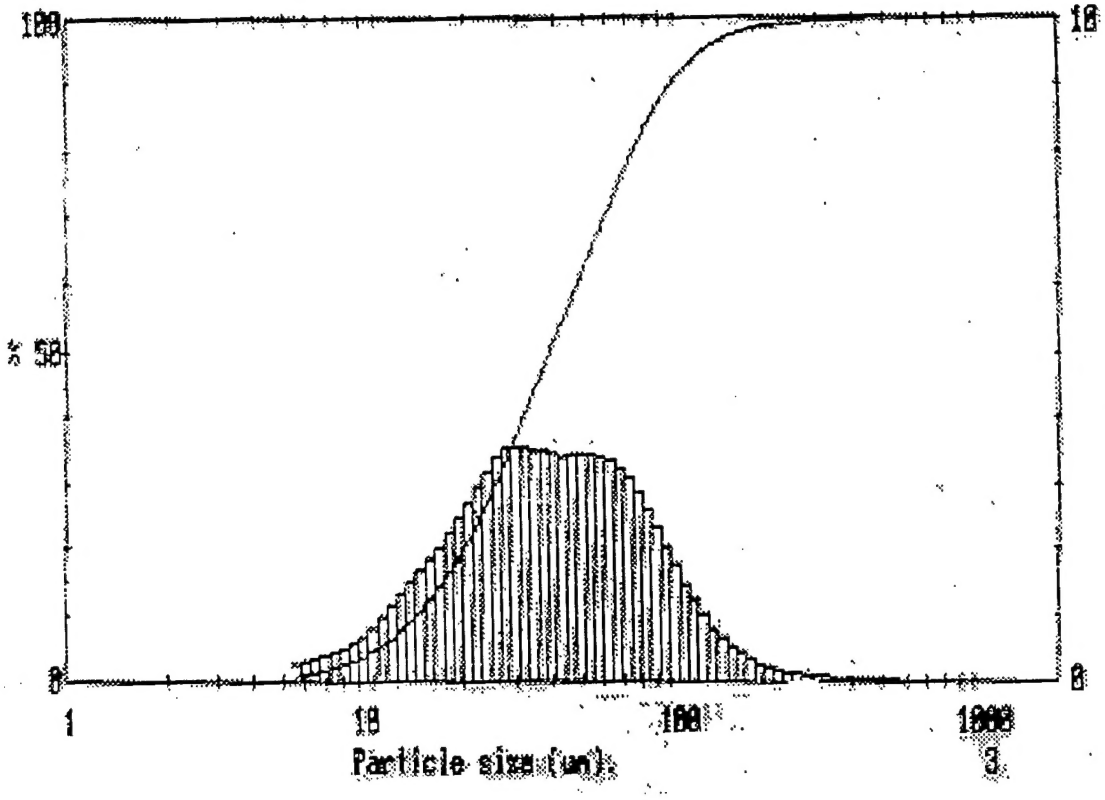

Figure A1: Size distribution of droplets leaving the oxidizer channel. Mist mass Fraction = 3%; SMD = 29μm.

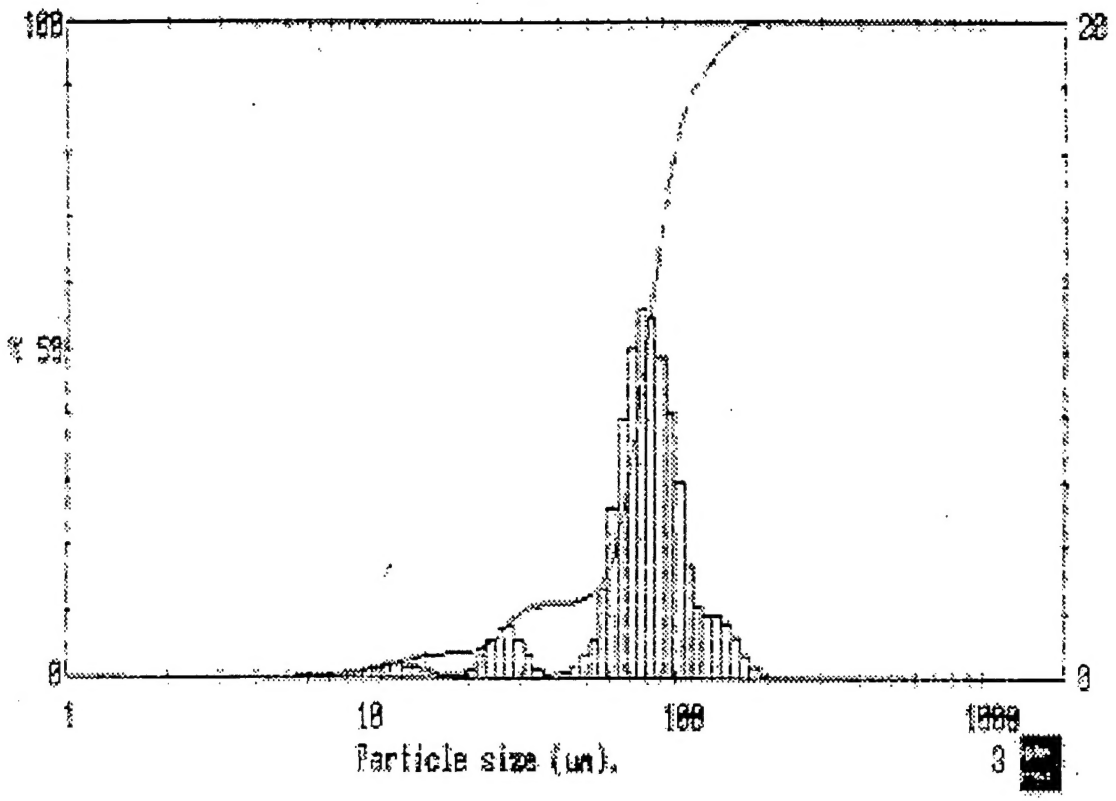

Figure A2: Size distribution of droplets leaving the oxidizer channel. Mist mass fraction = 5%; SMD = 54μm.

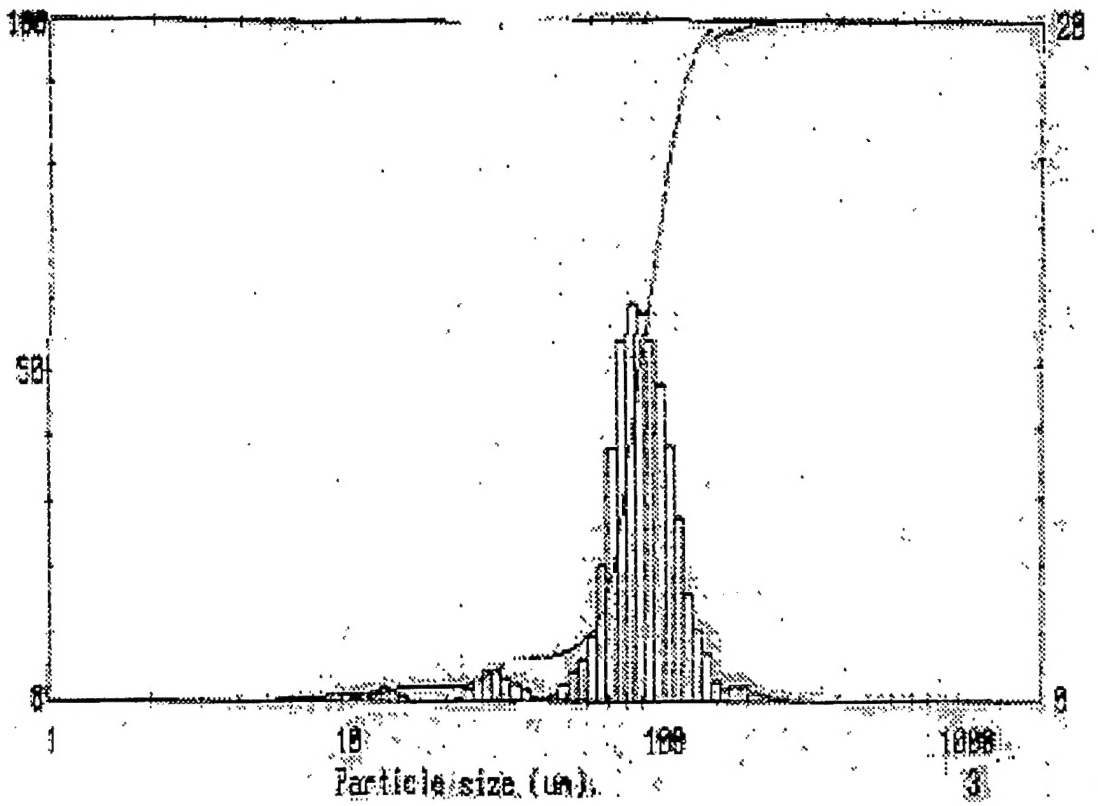

Figure A3: Size distribution of droplets leaving the oxidizer channel. Mist mass fraction + 7%; SMD = 66μm.